



UNIVERSITY OF LEEDS

This is a repository copy of *Multiscale Analysis Of A Migrating Submarine Channel System In A Tectonically-Confined Basin: The Miocene Gorgoglione Flysch Formation, Southern Italy*.

White Rose Research Online URL for this paper:  
<http://eprints.whiterose.ac.uk/129468/>

Version: Accepted Version

---

**Article:**

Casciano, CI, Patacci, M [orcid.org/0000-0003-1675-4643](https://orcid.org/0000-0003-1675-4643), Longhitano, SG et al. (3 more authors) (2019) Multiscale Analysis Of A Migrating Submarine Channel System In A Tectonically-Confined Basin: The Miocene Gorgoglione Flysch Formation, Southern Italy. *Sedimentology*, 66 (1). pp. 205-240. ISSN 0037-0746

<https://doi.org/10.1111/sed.12490>

---

© 2018 The Authors. *Sedimentology* © 2018 International Association of Sedimentologists. This is the peer reviewed version of the following article: Casciano, CI, Patacci, M, Longhitano, SG et al (2018). Multiscale Analysis Of A Migrating Submarine Channel System In A Tectonically-Confined Basin: The Miocene Gorgoglione Flysch Formation, Southern Italy. *Sedimentology*. which has been published in final form at <https://doi.org/10.1111/sed.12490>. This article may be used for non-commercial purposes in accordance with Wiley Terms and Conditions for Use of Self-Archived Versions.

**Reuse**

Items deposited in White Rose Research Online are protected by copyright, with all rights reserved unless indicated otherwise. They may be downloaded and/or printed for private study, or other acts as permitted by national copyright laws. The publisher or other rights holders may allow further reproduction and re-use of the full text version. This is indicated by the licence information on the White Rose Research Online record for the item.

**Takedown**

If you consider content in White Rose Research Online to be in breach of UK law, please notify us by emailing [eprints@whiterose.ac.uk](mailto:eprints@whiterose.ac.uk) including the URL of the record and the reason for the withdrawal request.



[eprints@whiterose.ac.uk](mailto:eprints@whiterose.ac.uk)  
<https://eprints.whiterose.ac.uk/>

# MULTISCALE ANALYSIS OF A MIGRATING SUBMARINE CHANNEL SYSTEM IN A TECTONICALLY-CONFINED BASIN: THE MIOCENE GORGOGNONE FLYSCH FORMATION, SOUTHERN ITALY

Casciano C.I.<sup>\*1</sup>, Patacci M.<sup>†</sup>, Longhitano, S.G.<sup>‡</sup>, Tropeano M.<sup>§</sup>, McCaffrey, W.D.<sup>†</sup>, Di Celma C.<sup>\*</sup>

<sup>\*</sup> Scuola di Scienze e Tecnologie, Sezione di Geologia, Università degli Studi di Camerino, Camerino, Italy

<sup>†</sup> Turbidites Research Group, School of Earth and Environment, University of Leeds, Leeds LS2 9JT, UK

<sup>‡</sup> Dipartimento di Scienze, Università della Basilicata, Potenza 85100, Italy

<sup>§</sup> *Dipartimento di Scienze della Terra e Geoambientali, Università degli Studi di Bari "Aldo Moro", Bari, Italy*

**Corresponding author's e-mail:** [claudio.casciano@unict.it](mailto:claudio.casciano@unict.it)

**<sup>1</sup>Present address:** Dipartimento di Scienze Biologiche, Geologiche e Ambientali – Sezione di Scienze della Terra, Università di Catania, 95129 Catania, Italy

**Short Title:** Multiscale analysis of a confined submarine channel system

## ABSTRACT

The Miocene Gorgoglione Flysch Fm records the stratigraphic product of protracted sediment transfer and deposition through a long-lived submarine channel system developed in a narrow and elongate thrust-top basin of the Southern Apennines (Italy). Channel-fill deposits are exposed in an outcrop belt approximately 500 m thick and 15 km long, oriented oblique to the paleoflow, which was roughly south-eastward. These exceptional exposures of channel-fill strata allow the stacking architectures and the evolution of the channel system to be analyzed at multiple scales, enabling the effects of syn-sedimentary thrust tectonics and basin confinement on the depositional system development to be deciphered. Two end-member types of elementary channel architecture have been identified: high-aspect-ratio, weakly-confined channels, and low-aspect-ratio, incisional channels. Their systematic stacking results in a complex pattern of seismic-scale depositional architectures that determines the stratigraphic framework of the deep-water system. From the base of the succession, two prominent channel-complex sets have been recognized, namely CS1 and CS2, consisting of amalgamated incisional channel elements and weakly-confined channel elements. These channelized units are overlain by isolated incisional channels, erosional into mud-prone slope deposits. The juxtaposition of different channel architectures is interpreted to have been governed by regional thrust-tectonics, in combination with a high subsidence rate that promoted significant aggradation. In this scenario, the alternating in- and out-of-sequence tectonic pulses of the basin-bounding thrusts controlled the activation of coarse-clastic inputs in the basin and the resulting stacking architectures of channelized units. The tectonically-driven confinement of the depositional system limited the lateral offset in channel stacking, preventing large-scale avulsions. This study represents an excellent opportunity to analyze the stratigraphic evolution of a submarine channel system in tectonically-active settings from an outcrop perspective. It should find wide

applicability in analogous depositional systems, whose stratigraphic architecture has been influenced by tectonically-controlled lateral confinement and associated lateral tilting.

**Keywords:** Submarine channels, thrust-top elongate basin, stacking pattern, syn-sedimentary thrust tectonics, basin structural confinement, Southern Apennines

## 1. INTRODUCTION

Coarse-grained sediments are generally transported into the deep-marine realm through an interconnected network of variously sized submarine channels (Mutti and Normark, 1987; Clark and Pickering, 1996; Peakall and Sumner, 2015). Commonly, channel architecture records a protracted history of incision and deposition at multiple scales related to different types of sediment-gravity flows (Hubbard et al., 2014). The main features of the sediment-gravity flows, such as magnitude and both density and type of transported sediment, may vary as a consequence of changes in allogenic (e.g., tectonics, sea-level fluctuations) and autogenic (e.g., channel avulsions) factors (Kneller, 2003; Pirmez et al., 2000; Sylvester and Covault, 2016; Jobe et al., 2016).

Despite the crucial role of submarine channels for the dynamics of sediment-routing systems and their importance as hydrocarbon reservoirs, the complex interactions between the mechanisms of sediment transport and the depositional architectures developed by the associated submarine channel systems remain poorly understood (Samuel et al., 2003; Porter et al., 2006; McHargue et al., 2011). Recent advances in seismic stratigraphy applied to conventional and high-resolution three-dimensional datasets offer a compelling method for understanding the large-scale geometries and stacking patterns of submarine channels (e.g., Mayall and Stewart, 2000; Posamentier and Kolla, 2003; Deptuck et al., 2003; Babonneau et al., 2010; Janocko et al., 2013). However, the spatial variability of reservoir properties is associated with small-scale differences in the nature of channel fills, occurring at scales below the resolution of 3D seismic datasets. For this reason, numerous studies have focused on the details of suitable outcrop analogues to improve the sub-seismic characterization of intra-channel stratal complexities (e.g., Navarro et al., 2007; Kane et al., 2009; Pyles et al., 2010; Thomas and Bodin, 2013; Li et al., 2016; 2018). In spite of their general 2D nature, the detailed characterization of outcrop analogues represents a powerful tool to resolve the internal anatomy of submarine channels, improving our knowledge on the sedimentary facies distribution and on the associated depositional processes (e.g., Beaubouef, 2004; Schwarz and Arnott, 2007; Di Celma, 2011; Figueiredo et al., 2013).

However, relating the observations made at the outcrop scale on ancient deep-water successions to the architectural styles of modern and subsurface deposits vividly imaged in seismic datasets can be challenging, mainly due to marked differences in resolution (Mutti and Normark, 1987; Deptuck et al., 2003; McHargue et al., 2011). Moreover, outcrop analogues are rarely extensive enough to allow for a broad-scale perspective of the depositional system (Beaubouef, 2004; Hodgson et al.,

2011; Van der Merwe et al., 2014). The Upper Miocene Gorgoglione Flysch (GF) Formation represents an exception to this common situation. This extraordinarily-preserved deep-water succession, deposited within a thrust-top basin of the Southern Apennines of Italy (Fig. 1), offers an excellent opportunity to investigate submarine channel architectures developed in tectonically active deep-water settings, from their small-scale facies architecture to their large-scale stacking pattern.

A primary objective of this study is to verify the predictability of the architectural geometries observed at the seismic scale (i.e., hundreds to thousands of meters) from the depositional features documented at the sub-seismic scale (i.e., centimeters to tens of meters). For this purpose, the stratal hierarchy of the deep-water system is explored through the detailed characterization of channel-fills and flanking out-of-channel deposits, and the interpretation of their spatial distribution across the outcrop belt. The effects of the basin configuration and syn-sedimentary thrust tectonics on the evolution of the depositional architectures are assessed. Finally, a model for deep-water sedimentation in elongate thrust-top basins is proposed, where the observed stratigraphic occurrence of different architectural styles is interpreted to reflect a progressive shift of the deep-water system along the depositional profile. This model should find wide applicability in other basins, particularly those formed along active margins, in regions where deep-water channel systems developed in tectonically-confined settings.

## **2. STUDY AREA AND GEOLOGICAL SETTING**

The Southern Apennines are a prominent thrust-and-fold belt developed from late Oligocene to Pleistocene on a W-dipping subduction zone, in the general framework of African and Eurasian major plates convergence (Gueguen et al., 1998; Patacca and Scandone, 2007). The resulting north-eastward migration of the orogenic thrust front determined the progressive involvement in the thrust belt of the intervening Meso-Cenozoic basin and platform successions covering the Adria passive margin and the adjacent Tethyan ocean (Patacca and Scandone, 2007 and references therein). Accordingly, the structure of the Southern Apennine accretionary wedge is configured as a thick pile of deformed rootless nappes, tectonically overlying a buried deep-seated carbonate duplex system (Vezzani et al., 2010 and references therein).

Syn-tectonic thrust-top basins of upper Eocene to Plio-Pleistocene age, were progressively filled by coarse-clastic sediments derived from the emerged areas of the chain, unconformably covering the whole thrust-pile (Patacca and Scandone, 2007; Vezzani et al., 2010). One of the better-preserved thrust-top depositional units of the Southern Apennines is the Gorgoglione Flysch (GF) Formation, an approximately 2 km thick deep-water succession that crops out in the eastern sector of the thrust belt. Main exposures of the GF succession occur in two broad areas, 150 km SE of Naples, in southern Italy (Fig. 1). Along the eastern edge of the former turbidite basin, the GF succession unconformably overlies the Cretaceous-Eocene mud-rich units of the Argille Varicolori Formation,

which represents the deformed substrate (Fig. 1; Boiano, 1997). The deep-water strata of the GF succession consist of coarse-grained sandy turbidites and mudstones with subordinate conglomerates, forming a prominent channel system developed within a narrow and elongate, NNW-SSE-trending basin (Boiano, 1997), oriented nearly parallel to the mean trend of Apennine thrust faults (Fig. 1). Basin physiography and evolution of its sedimentary fill were controlled by the contractional tectonics affecting the Southern Apennine accretionary wedge during the late Miocene (Pescatore, 1978; 1988). The deep-water succession was deposited from the late Burdigalian to the Tortonian (Maffione et al., 2013; Giannandrea et al., 2016), with variable degrees of lateral confinement, provided by the growing orogen to the W and by the incipient outer thrust structures of the thrust-and-fold belt to the east (Pescatore et al., 1999; Butler and Tavarnelli, 2006). Provenance data show that the GF was sourced from a crystalline basement terrane located within the orogenic hinterland to the west (Critelli and Loiacono, 1988; Critelli et al., 2017). However, paleocurrent indicators document a prevalent paleoflow direction from NNW to SSE, along the longitudinal axis of the basin (Loiacono, 1974). Accordingly, many authors invoked a paleogeographic scenario with sediment-gravity flows originated from a shelf to the west, which were directed down a NE-facing slope and successively deviated near the base-of-slope toward SSE, along the basin axis (Pescatore and Senatore, 1986; Butler and Tavarnelli, 2006).

In this study, the seismic-scale architecture and the outcrop-scale depositional features of the GF succession have been investigated across an outcrop belt approximately 500 m high and 15 km long, exposed near the towns of Pietrapertosa and Castelmezzano (Fig. 2A). The study area, located in the northern sector of the GF basin, is characterized by a well-exposed monoclinical structure, dipping SW by approximately 40°, which defines an extensive ridge oriented obliquely to the main sediment dispersal direction and resulting in the apparent elongate shape of the depositional units (Fig. 2B). The outcrop belt orientation slightly changes from north to south of the study area: north of Castelmezzano, it is oriented N-S, while south of Pietrapertosa its orientation is NW-SE. This variable configuration of the outcrop belt allows the observation and reconstruction of the lateral variability of the main sandbodies. The monocline represents the eastern flank of a NNW - SSE trending syncline (Fig. 1) in which the GF formation was deformed during the post-Tortonian contractional tectonic phase of the Southern Apennines (Cavalcante et al., 2015).

### **3. METHODOLOGY**

The deep-water strata of the GF system have been studied using both standard sedimentary facies analysis and digital field techniques, such as high-resolution photomosaics and structure-from-motion (SFM) 3D photogrammetry (Pitts et al., 2017). Traditional methods included bed-scale characterization of sedimentological and stratigraphic elements and paleoflow analysis. Twenty-four main stratigraphic sections were measured at cm to dm-scale (Fig. 2A) to document key sedimentary

features such as lithology, grain-size and sorting, primary sedimentary structures, bedding thickness and the nature of bed contacts, which form the basis for facies analysis. The distribution of the strata is documented in a geological map of the study area (Fig 4), which illustrates the main depositional architectures. In order to characterize lateral changes in stratigraphic architecture over variable distances, the lateral spacing between the stratigraphic sections ranges between 30 and 750 m. Logging was performed using a meter-scale folding-tape measure and a 2.1 m high Jacob's staff, instrumented with an integrated laser pointer, which allowed an improved accuracy in thickness measurements (Patacci, 2016). Paleoflow data were recorded across the entire outcrop belt from 936 paleoflow indicators, such as sole marks, ripple-marks, and cross-stratification (Fig. 5). The sedimentary log data were compiled into a database. For each bed, these data included thickness, stratigraphic height of base and top, lithology, facies type, grain-size and paleocurrent type and direction. This dataset allowed an array of secondary parameters to be determined, such as sandstone-to-mudstone ratio, and bed thickness trends. Pie charts of facies abundance were employed to contrast different stratigraphic intervals of the studied sections and to compare their facies distribution.

Additional digital data collection methods included the construction of ultra-high-resolution outcrop panoramas produced by the GigaPan® imagery system and 3D outcrop models produced from aerial and ground based imagery using SFM 3D photogrammetry, built to aid in the identification of key surfaces and to improve the analysis of depositional architectures (Pitts et al., 2017). Where possible, key stratigraphic surfaces have been walked and mapped using a GPS to improve their spatial reconstruction.

#### **4. FACIES ASSOCIATIONS AND DEPOSITIONAL ELEMENTS**

The GF deep-water succession consists of a wide range of sedimentary facies, which have been distinguished on the basis of sedimentological criteria (Bouma, 1962; Allen, 1963; Lowe, 1982; Larue and Provine, 1988; Mutti, 1992; Kneller and McCaffrey, 2003; Talling et al., 2012) and are described and interpreted in Table 1. The sedimentary facies include: (i) Extra- and intra-formational conglomerates encompassed within a coarse-grained sandstone matrix (LF1; Fig. 3A, B); (ii) Structureless, commonly amalgamated, coarse-grained sandstones (LF2; Fig. 3C, D); (iii) Structured, coarse-grained deposits, including planar-laminated sandstones (LF3; Fig. 3E) and cross-stratified sandstones (LF4; Fig. 3F); (iv) A wide spectrum of thin-bedded, "classical" Bouma-type turbidites (from LF5 to LF10; Fig. 3G, H, I, L, M, N); (v) Deformed and contorted sandstone beds (LF11); and (vi) Mudstones (LF12).

The composition of sandstones and conglomerates is quartzo-feldspathic, indicating a source dominated by granitic and gneissic metasedimentary rocks, carbonatic and siliceous sedimentary rocks, and minor felsitic and silicic volcanics (Critelli and Loiacono, 1988; Critelli et al., 2017). The

textural and compositional immaturity of the GF sandstones has been associated with a rapid erosion of the source-rock and a general high sedimentation rate in the basin (Critelli and Loiacono, 1988).

The sedimentary facies represent the basis for the interpretation of the various modes of sediment deposition. Based on their spatial arrangement and depositional features, three facies associations have been identified.

#### 4.1. Facies association 1 (F.A.1) - Sandy and gravelly amalgamated deposits

Description. F.A.1 is characterized by a systematic distribution of vertically-stacked coarse-grained facies arranged in a crude fining-upward trend, commonly overlying prominent concave-upward erosion surfaces (Fig. 6). These facies include: a basal, matrix-supported conglomerate (LF1), grading upward into thick, structureless amalgamated sandstones (LF2) and planar-laminated sandstones (LF3), abruptly capped by multiple orders of large-scale cross-stratified sandstones (LF4) or by thick packages of structured, fine-grained sandstones (LF6 and LF8) and subordinate massive sandstones (LF5). The proportions of these facies are highly variable between the studied sections where F.A.1 has been documented, with some components locally reduced or even missing. Single F.A.1 sediment packages are typically characterized by slightly undulated tops and sharp concave-upward bases producing roughly lenticular geometries. Extraformational conglomerates (LF1A) and amalgamated, thick-bedded structureless sandstones with sparse granule- to pebble-sized clasts (LF2B) typically characterize the thickest portions of F.A.1 sandbodies (Fig. 6A). Abundant LF1A conglomerates are commonly confined within the deepest portions of the basal erosion surface. Their abundance decreases laterally along the basal surface, gradually being replaced by thick intervals constituted solely by intra-formational mudstone breccias (LF1B). Amalgamated LF2B sandstones typically exhibit a lateral transition to thinner and less amalgamated, clean massive sandstones (LF2A) and plane-parallel laminated sandstones (LF3) alternating with thin mudstone beds (LF12), which have been locally documented to onlap the basal erosion surface of the sandbodies.

The primary basal surfaces commonly exhibit steep notches, which produce a stepped cross-sectional geometry (Fig. 6A, B), and are locally ornamented by sole structures up to 20 cm long and minor loading features (Pitts et al., 2017). Paleocurrent measurements from these basal indicators across the study area reveal an average flow towards 149°, ranging from 100° to 206° (Fig. 5), consistent with the regional dispersal pattern reported by Loiacono (1974) and Boiano (1997). Subordinate erosion surfaces mantled by LF1 conglomerates are widely documented within the primary basal surfaces, truncating the underlying coarse-grained beds of F.A.1.

Interpretation. Based on the three-dimensional arrangement of the coarse-grained facies, F.A.1 sandbodies have been attributed to processes of erosion, sediment bypass and ultimately filling of submarine channels (e.g., Mutti and Normark, 1987; Gardner and Borer, 2000). Concave upward

basal surfaces were sculpted by multiple incisional gravity flows that passed through the channel and transported much of their sediment load basinward, leaving behind chaotic conglomerate-rich lag deposits (LF1) that drape the channel base (Barton et al., 2010). Matrix-supported conglomerates dominate the channel axis and off-axis and denote the substantial erosion and sediment bypass that affected these portions of the channel forms (Hubbard et al., 2014; Stevenson et al., 2015). Abundant extra-formational conglomerates (LF1A) are interpreted to characterize the channel axis setting (e.g., Camacho et al., 2002) and to indicate the channel thalweg (Thomas and Bodin, 2013). Conversely, their absence associated with a corresponding increase of intra-formational mudclast conglomerates (LF1B; Fig. 6B), suggests deposition within a channel off-axis setting (Hubbard et al., 2014). Intra-formational mudstone clast breccias are commonly attributed to “rip-up” processes, as mudclasts are incorporated into the bypassing flows after turbulent scouring of the substrate (Butler and Tavarnelli, 2006).

Secondary erosion surfaces draped by conglomeratic lags are particularly well developed in the channel axis. These subordinate surfaces are suggestive of short-lived periods of flow bypass or erosion punctuating the main channel-fill phase (Beaubouef et al., 1999; Campion et al., 2005; Stevenson et al., 2015).

Channel-axis stratigraphy is dominated by amalgamated LF2B sandstones (Fig. 6A), resulting from rapid deposition by collapsing sand-rich high-density turbidity currents (e.g., McCaffrey and Kneller, 2004; Hubbard et al., 2014). Conversely, the channel margins are interpreted to be characterized by less amalgamated LF2A and LF3 sandstones with intervening mudstones. The character of this lateral transition from channel axis to margin facies is variable across the different channelized units of the GF succession and has been crucial to classify the different types of channel architectures.

In the channel margin setting, the limited occurrence of internal erosion surfaces, together with poorly developed sole structures, indicates that sediment-gravity flows were only partially erosive. However, the presence of LF2A sandstones associated with high fall-out rates from high-density turbidity currents (Lowe, 1982), suggests that these flows were rapidly declining from erosional to depositional (Li et al., 2016).

Large-scale, cross-stratified deposits (LF4) capping the channel-fill successions (Fig. 6C) have been interpreted to record the final phases of channel infill, with the progressive reduction of channel confinement leading to the formation of relatively fast and dilute, fully turbulent flows. Multiple orders of superimposed cross-sets record a variable range of paleocurrent directions, diverging up to 75° from the mean paleoflow determined by the sole structures beneath channel-fill packages. These divergent paleoflow trends are consistent with a partial lateral flow expansion as channel confinement progressively decreases. On the other hand, the infilling of the channel is typically symptomatic of decreasing flow magnitude and energy (Hubbard et al., 2014), with the cross-stratified deposits that might have recorded this transition. The different large-scale cross sets at the

channel top can be related to the final channel filling by three-dimensional bedforms, as invoked by Brunt and McCaffrey (2007) for the submarine channels of the Grès du Champsaur (southern France). Within the GF channels, the progressive compensation of the channel top irregularities by multiple stacked three-dimensional bedforms might have resulted in distinct superimposed orders of cross-sets with different paleoflow directions.

Where the capping cross-stratified interval is absent, the upper portion of channel-fill successions comprises abundant planar-laminated and ripple cross-laminated, fine-grained sandstones (LF6 and LF8, respectively) and subordinate massive sandstones (LF5) alternating with mudstones (Fig. 6D). These facies and the upward decrease in the degree of amalgamation suggest a progressive decline in sand proportions, volume and energy of the flows in the channel conduit (Hubbard et al., 2014).

#### 4.2. Facies association 2 (F.A.2) - Sand-prone, heterolithic deposits

**Description.** The F.A.2 (Fig. 7A) typically flanks the channel-fill deposits, showing a progressive upward and lateral transition into mud-prone thin-bedded heterolithic deposits of facies association 3 (F.A.3). They consist of alternating thin- to medium-bedded sandstones (facies LF5 to LF10) and mudstones (LF12), with occasional folded and contorted deposits (LF11), organized in well-stratified packages (Fig. 7A) up to 75 m thick. Across the study area, these deposits have been documented outside the primary erosion surfaces confining F.A.1 packages, being locally incised by them (Fig. 8). Paleocurrent indicators typically suggest variable flow directions, with the dominant flow being obliquely away from the adjacent F.A.1 package (Fig. 8). Massive Ta-dominated beds (LF5), represent about 40% of the total F.A.2 volume, with subordinate Tb - and Tc-dominated beds (LF6 and LF8, respectively; Fig. 4B). Sandstone beds range from 10 to 70 cm thick and are typically tabular, showing a rather constant bed thickness at the outcrop scale (ca. 100 m). Bed bases are commonly flat or weakly erosive into the underlying mudstones. Bed amalgamation is rare. Sandstone beds are abruptly overlain by thin (1–5 cm) layers of mudstone (LF12), which constitute around 16% of F.A.2 packages (Fig. 4B).

**Interpretation.** The sedimentological features of F.A.2 packages might be consistent with deposition in channel off-axis or margin positions (e.g. Hubbard et al., 2014). In these intra-channel settings, the thinly interbedded sandstone and mudstone facies are confined within primary channel surfaces and onlap against them (Pringle et al., 2010; Kane and Hodgson, 2011), showing a rapid transition to amalgamated sandstones laterally, towards the channel axes (Deptuck et al., 2003; Di Celma et al., 2013; Hubbard et al., 2014). However, in the GF succession, this type of lateral transition from thin bedded F.A.2 deposits to thick bedded sandstones of F.A.1 has not been observed within the channelforms. Conversely, the stratigraphic distribution of F.A.2 deposits adjacent and among the amalgamated paleo-channelized bodies (Fig. 4), but outside primary channel confinements, suggests overbank deposition by widespread, moderate- to low-concentration turbidity currents

overflowing an active channel (Hansen et al., 2015). The occurrence of substantial F.A.2 packages up to 75 m thick, which do not show any evidence of large channelform surfaces, and the wide range of paleoflows diverging from the measurements in the adjacent channel-fill deposits (Figs. 5, 8) are consistent with this interpretation (Kane et al., 2010). F.A.2 overbank deposits are relatively sand-rich. The relative abundance of massive LF5 sandstones, together with little evidence of erosion and bed amalgamation within F.A.2 packages, suggest an overbank position proximal to the associated channel (Kane et al., 2007; Migeon et al., 2012).

#### 4.3. Facies association 3 (F.A.3) - Mud-prone heterolithic deposits

**Description.** Thin-bedded packages of alternating fine- to very-fine-grained sandstone beds and mudstone or siltstone beds characterize F.A.3 packages (Fig. 7B). Mudstone or siltstone intervals of facies LF12 are dominant, representing about 60% of the total F.A.3 (Fig. 4B) with an average thickness of c. 10 cm, occasionally up to 30 cm. Sandstone beds are typically up to 6 cm thick and consist mainly of abundant ripple cross-laminations or mm-thick parallel laminations (LF8 and LF6, respectively). Massive sandy beds of facies LF5, up to 50 cm thick and weakly erosional into the muddier substrate, locally occur within the mud-prone packages, displaying lenticular geometries at the scale of the tens of meters (Fig. 7B). F.A.3 packages may reach considerable thicknesses (i.e., > 100 m) in the upper part of the GF succession, where they are deeply incised by isolated F.A.1 sandbodies. As for the F.A.2 deposits, F.A.3 strata have not been documented within primary channelform surfaces, neither draping them nor towards the margins of the channelforms.

**Interpretation.** The sedimentological features of the mud-prone heterolithic deposits could be explained by a number of alternative depositional models. They could represent: (i) intra-channel deposits, such as bypass drapes mantling primary channel surfaces (Alpak et al., 2013) or channel margin facies (Hubbard et al., 2014); ii) channel-overbank strata (e.g., Kane and Hodgson, 2011); or iii) background slope deposits, occasionally incised by slope channels (e.g., Figueiredo et al., 2010).

Fine-grained facies may occur within channelform surfaces as a result of different sedimentary processes. Bypass drape deposits are considered as the product of traction and fallout of the fine-grained tail of largely bypassing high-density flows transiting through the channel conduits (Mutti and Normark, 1987; Stevenson et al., 2015). On the other hand, fine-grained channel-margin facies are attributed to the low energy experienced by gravity flows traversing submarine conduits towards the margins of the original channel incision (McHargue et al., 2011; Macauley and Hubbard, 2013). In the GF succession, however, the typical occurrence of very-thick packages of F.A.3 strata outside the primary channel confinements suggests that their interpretation as intra-channel deposits is unlikely.

In the second scenario (i.e., channel-overbank strata), the deposition of thick, mud-dominated packages can be interpreted to result from far-travelling and dilute over-spilling turbidity currents that reached distal overbank areas having deposited most of their coarser-grained sediment load in more proximal overbank areas (Kane et al., 2007). Alternatively, mud-prone overbank deposits may also result from the substantial overspill of the upper, more dilute portion of highly-confined flows traversing the channels (Hiscott et al., 1997; Arnott et al., 2011).

Thin sandstone beds might also have been deposited by volumetrically small and dilute, low-density turbidity currents typically occurring in slope environments (e.g., Figueiredo et al., 2010; Bayliss and Pickering 2015b). Lenticular beds of facies LF5 can be interpreted as shallow scour-fill deposits, indicating fluctuations in the volumes of turbidity flows. The considerable thickness of F.A.3 packages in the upper part of the GF succession, without any internal depositional trend, are consistent with this interpretation.

## **5. ARCHITECTURAL AND SEDIMENTOLOGICAL VARIABILITY**

### **5.1. Channel hierarchy**

In the study area, due to their heterolithic and relatively fine-grained nature, F.A.2 and F.A.3 deposits commonly weather recessively and are often covered by vegetation. In some locations, however, very thick packages of these heterolithic deposits crop out, allowing their detailed characterization. Conversely, channel-fill deposits of F.A.1 crop out extensively, forming spectacular cliffs (Fig. 2B) that allowed the detailed architectural characterization of the channelized units. For this purpose, a hierarchical approach is essential, facilitating the recognition and interpretation of persistent patterns at multiple scales (e.g., Ghosh and Lowe, 1993; Di Celma et al., 2011; Macauley and Hubbard, 2013; Stright et al., 2014). Hierarchical classifications are crucial to assign spatial and temporal order to the sedimentary architecture of preserved deep-marine deposits and to genetically related modern landforms (Cullis et al., 2018). The stratigraphic hierarchy used in this study is based on the schemes proposed by Campion et al. (2005).

The fundamental building blocks of submarine channel systems is the channel element. Individual elementary channels define distinct conduits for relatively confined flows and are commonly dissected by secondary erosion surfaces bounding discrete fill phases, called “stories”, that are up to 5 m thick. The vertical or horizontal stacking of multiple, genetically-related channel elements with similar architectural style and lithofacies organization constitute a single channel complex. These architectural units in the GF succession are up to 85 m thick, comparable to other channel complexes documented in literature (e.g., Stright et al., 2014; Bain and Hubbard, 2016). Where multiple genetically-related channel complexes are stacked in a consistent pattern, they form a single channel complex-set. In this study, the recognized channel complex-sets are approximately 100 to 300 m in

thickness. Comparable dimensions have been reported by Beaubouef (2004) in the Cerro Toro Formation (Magallanes Basin, Chile) and Thomas and Bodin (2013) in the Finale channel system of the Numidian Flysch Formation (Sicilide Basin, southern Italy).

## 5.2. Elementary channel architectures

The distribution of the channel-fill facies, together with the nature of their flanking out-of-channel deposits and the geometry of the channelforms, show a substantial variability across the study area. Based on these observations, two end-member types of elementary channel architectures have been recognized: weakly-confined channels and incisional channels (Fig. 9 and Table 2). In the analysis of elementary channel architectures, while channel thicknesses were easily measured through sedimentological logs, direct measurements of strike-oriented channel widths were difficult due to the oblique orientation of the outcrop belt relative to the paleoflow. However, local outcrop sections oriented perpendicularly to the main paleoflow direction offered opportunities to collect information about channel widths. Moreover, for some elementary channel units, the widths have been calculated for reconstructed strike-oriented cross sections by projecting the apparent dimensions onto a surface normal to the average paleocurrent direction (Fig. 9; Pitts et al., 2017).

### 5.2.1. Weakly-confined channels

These channelized sedimentary bodies are typically 5–17 m thick, occasionally up to 20 m, and have widths of > 450 m, resulting in aspect ratios higher than 50 (Table 2 and Fig. 9A). Weakly-confined channels display geometries similar to those described by Brunt et al. (2013b) in the Unit B of the Laingsburg Formation (Karoo Basin, South Africa). Amalgamated LF2B sandstones are prevalent within the channel axes, but less amalgamated, thick bedded LF2A and LF3 sandstones and intervening mudstones become dominant towards the channel margins, directly overlaying the primary channelform surfaces, with some beds onlapping the channel base. Basal channel surfaces are mantled exclusively by thick packages of matrix-supported mudclast conglomerates (LF1B), with rare extra-formational conglomerates (LF1A), and show a significant decrease in erosional character towards the marginal areas of the channelform.

The axis to margin facies transition and the poorly-erosional nature of the basal surfaces at the margins suggest relatively high energy levels in channel axes and progressively lower energy levels towards marginal areas (Navarro et al., 2007; Pemberton et al., 2016). Flows traversing weakly-confined channels are interpreted to have been larger than the axial confinement. These flows overspilled their initial lateral confinement (Brunt et al., 2013b) and formed proximal sand-rich overbank deposits (F.A.2) that progressively aggraded (Arnott et al., 2011). Overbank aggradation slightly increased the confinement of the large turbidity flows, with a progressive reduction of the volume of overspill that resulted in thinning-upward trends (e.g., Kane et al., 2007; Kane and Hodgson, 2011),

locally documented within F.A.2 heterolithic packages (Fig. 7A). Similar channel architectures have been interpreted by Stevenson et al. (2013) as the product of largely unconfined flows passing across low sinuosity channels. The narrow paleocurrent dispersion in the weakly-confined channels of the GF succession, compared to the large variability of paleoflow directions measured from the adjacent F.A.2 deposits, seem to corroborate this interpretation (Fig. 5).

### 5.2.2. Incisional channels

In the studied succession, the fill of incisional channels are typically 13–26 m thick and 180–450 m wide, with aspect-ratios between 10 and 30 (Pitts et al., 2017; Table 2 and Fig. 9B). These dimensions are consistent with low-aspect-ratio slope channels reported in literature for other deep-water systems (McHargue et al., 2011). Incisional channel fills display a multistorey architecture (Fig. 9B) and are relatively coarser-grained than weakly-confined channels. Amalgamated LF2B sandstones dominate the majority of channel element's infill, with subordinate, less amalgamated LF2A sandstones and intervening mudstone beds only relegated towards the edges of the channelform surface. Incisional channels are commonly flanked by, and deeply incisional into, thick packages of mud-prone heterolithic deposits of F.A.3.

The spatial distribution of the channel-fill facies and the fine-grained nature of the out-of-channel deposits are indicative of high-energy incisional flows carving deep erosional conduits and becoming strongly confined by the resulting morphologies (e.g., Brunt and McCaffrey, 2007; Hubbard et al., 2014; Pemberton et al., 2016).

### 5.3. Seismic-scale architectural units

The distribution of incisional and weakly-confined elementary channels effectively controls the depositional architectures developed by the large-scale channelized units of the GF system (Fig. 10). In the study area, two prominent channel complex-sets have been recognized: CS1 and CS2 (Fig. 10), composed of multiple stacked and amalgamated channel complexes, laterally associated with thick sand-prone (F.A.2) and mud-prone (F.A.3) heterolithic deposits. CS2 is directly overlain by isolated channels and channel complexes, representing the dominant architectural unit in the upper portion of the deep-water succession, where they are incised into F.A.3 mud-prone heterolithic deposits.

These architectural units are described from the base to the top of the GF succession, including their location, large-scale lithological variability and main internal stratigraphic surfaces, as well as other notable characteristics that support paleo-environmental interpretations. Detailed characterization of the architectural units, together with the reconstruction of their stratigraphic relationships, is crucial to the interpretation of the evolutionary history of the GF deep-water system. Of the different

mappable sandstone units present in the GF succession (Figs. 4, 7B), CS2 is the best exposed and least disrupted by post-depositional features.

### 5.3.1. Channel complex-set 1 (CS1)

Description. CS1 is an isolated channel complex-set that crops out at the base of the GF succession, in an area located at confluence of the Basento River and Caperrino Creek (Figs. 4, 10). In map view, CS1 outcrops have an irregular shape, elongated in NE-SW direction as a result of the oblique orientation of the outcrop belt to the main paleoflow trend, with a maximum lateral extension of approximately 1200 m measured along strike (Fig. 4).

Channel-fill strata dip towards NW at approximately 70°, showing a comparatively higher dip-angle than those of CS2, which dip towards NW at about 40°. CS1 unconformably overlies the clayey units of the Argille Varicolori Formation along an extensive, irregularly-shaped stratigraphic surface (Fig. 4; Piedilato and Prosser, 2005), which locally cuts down for tens of meters into the underlying sediments.

This channel-complex set reaches a maximum thickness of nearly 100 m, resulting from the amalgamation and stacking of several F.A.1 packages. Thick beds of abundant matrix-supported extrabasinal conglomerates (LF1A), directly overlying concave-upward erosion surfaces, grade upward into amalgamated coarse-grained, poorly-sorted sandstones of facies LF2B. Single F.A.1 units are up to ~10 m thick, but are deeply truncated by the erosional surface at the base of the overlying F.A.1 package. Paleoflow indicators were not observed in this stratigraphic unit due to the amalgamation of the component sandbodies and to the lack of suitable exposures.

CS1 is flanked by thinly-bedded, mud-prone heterolithic deposits of F.A.3, with the outcrop extending laterally for about 7 km towards SE and about 3 km towards NW (Fig. 4). Moreover, a nearly 100 m thick package of F.A.3 deposits occurs above CS1, separating it from the base of CS2 (Fig. 4).

Interpretation. Previous studies interpreted the deposition of CS1 coarse-grained sediments as the progressive infill of topographic irregularities on the basin floor (Loiacono, 1993; Boiano, 1997). However, the incisional nature of the irregular basal surface that truncates the underlying units of the substrate for tens of meters might suggest an erosional origin for CS1. It is possible that incisional flows might have used the topographic irregularities of the muddy substrate as templates for the subsequent development of channelized architectures (e.g., Fildani et al., 2013).

Bed-scale observations on the sedimentological and architectural features of the preserved F.A.1 packages indicate that CS1 consists of multiple stacked and amalgamated, incisional channel elements. The considerable abundance of LF1A conglomerates and subordinate poorly-sorted LF2B sandstones suggests that the axes of these highly incisional channels are predominantly exposed, which show significant evidence of sediment bypass (Stevenson et al., 2015).

### 5.3.2. Channel complex-set 2 (CS2)

Description. CS2 crops out throughout the study area for up to 11.5 km, albeit with local discontinuous exposures (Fig. 2B). It consists of two broad channel belts, named CS2A and CS2B. The lower of the two channel belts (i.e., CS2A) overlies an extensive erosion surface, carved into the underlying mud-prone deposits. At the large-scale, the outcrops of these channel belts show a pronounced elongated geometry in NNW-SSE direction, highly oblique to the main paleoflow direction, and converge towards the north (Fig. 4), although the locus of the conjunction is not exposed. In the opposite direction, towards SSE, both of them display a progressive thinning, passing from a maximum thickness of 330 m north of the Castelmezzano village to ~35 m south of the Pietrapertosa village (Fig. 4).

CS2A and CS2B display similar sedimentological features and are characterized by a composite architecture, resulting from the amalgamation of several F.A.1 sandbodies, laterally associated with sand-prone F.A.2 heterolithic deposits. Individual packages of F.A.1 sandstones are 6 to 19 m thick and display clear channelized architectures, overlaying irregular, concave-upward basal surfaces (Figs. 9A, 11). These sandbodies define individual channel elements, which stack to form 60-85 m thick channel complexes demarcated by major erosion surfaces that can be traced longitudinally for up to 4 km, as documented within the superbly exposed cliffs of CS2B (Fig. 12). In its northern sector, four amalgamated, partially off-set stacked channel complexes have been recognized (Fig. 12). Here, the component channel elements are 15-19 m thick and display local widths of > 450m (Fig. 9A), with the exposed channel-fills dominated by amalgamated poorly-sorted LF2B sandstones and LF1B mudclast-rich conglomerates draping the basal surfaces (Fig. 13). These deposits grade laterally into less amalgamated, clean massive sandstones (LF2A) and planar laminated sandstones (LF3) overlying weakly erosional surfaces, which locally provide complete perspectives of the channel widths (e.g., Fig. 9A). Channel complexes gradually thin towards SE, where increasingly thicker packages of sand-prone heterolithic deposits (F.A.2) occur and separate into individual channelized units (Fig. 13). Further towards SE, amalgamated channel-fill deposits pass laterally into lenticular sandbodies, 6-15 m thick and laterally-persistent for up to 600 m (Figs. 4, 13). These sandbodies are essentially comprised of thick-bedded, partially amalgamated LF2A and LF3 sandstones, directly overlying and onlapping weakly-incisional basal surfaces, and are capped by large-scale cross stratified sandstones (LF4). A similar lateral transition from amalgamated coarse-grained sandstones into extensive lenticular sandbodies has been also documented towards north, in the upper part of the CS2B (Figs. 4, 13). Paleoflow indicators are limited compared to those documented from the isolated channels in the upper part of the succession (Fig. 5). However, sole marks at the base of the amalgamated sandbodies in CS2B indicate average flow to SE (159°), ranging from 100° to 232°, whereas indicators (i.e., ripples and sole structures) from the adjacent heterolithic deposits reveal a wider range of paleoflow directions, spanning from E to SW (Fig. 5).

The cross-stratified sandstones at the top of CS2B sandbodies are instead characterised by multiple orders of superimposed cross-sets recording paleocurrent directions that diverge up to 75° from the average paleoflow measured from the basal indicators.

Interpretation. Due to their lateral extension, CS2A and CS2B represent important stratigraphic markers in the GF succession (Boiano, 1997). Previous workers interpreted them as two distinct systems, relating their formation to the combined effect of eustatic sea-level fall and basin modifications associated to thrust tectonics (Loiacono, 1993; Boiano, 1997; Giannandrea et al., 2016). However, the convergence of the two channel belts observed in the northern sector of the study area (Fig. 4), together with their analogous sedimentological features, are indicative of architectural continuity and suggests that CS2A and CS2B represent a single channel complex-set, the CS2, characterized by a systematic aggradation and lateral migration of its component units.

The depositional style displayed by CS2 could be the result of multiple phases of allocyclically-driven seafloor degradation and aggradation (e.g., Deptuck et al., 2003; Hodgson et al., 2011) through the protracted evolution of weakly-confined channel elements, as suggested by the sedimentological features of the amalgamated sandbodies documented in this stratigraphic interval. Individual elementary channels stack to form channel complexes bounded by composite, longitudinally-extensive basal surfaces, likely resulting from multiple erosion and infill phases associated with high-energy turbidity currents (e.g., Eschard et al. 2003; Beaubouef, 2004). The occurrence of numerous stacked and amalgamated channel elements (Fig. 11) is commonly identified as evidence for prolonged sediment transfer (e.g., Di Celma et al., 2011; Sylvester et al., 2011).

In this scenario, the prominent erosion surface at the base of CS2A can be interpreted as the record of the master channel complex-set conduit (*sensu* Macauley and Hubbard, 2013; erosional valley surface *sensu* McHargue et al., 2011; submarine incised valley *sensu* Janocko et al., 2013) confining the CS2. However, due to the high obliquity of the outcrop belt that mainly provides a longitudinal perspective of the master conduit geometry, the different processes active during the establishment of the master conduit (e.g., down-cutting, mass failure, external levee construction) cannot be ascertained from the available dataset.

The reported dimensions and the spatial distribution of the channel-fill facies across CS2B (Figs. 9A, 13) suggest that, in the northern sector of the channel belt, the axes of the amalgamated, weakly-confined channels widely crop out, with only limited exposures of their channel margins. Towards the SE, these amalgamated channels show a gradual transition to laterally-persistent, lenticular sandbodies (Figs. 4, 12), which are interpreted to represent the margins of the stacked weakly-confined channels. It seems likely that in the south-eastern portion of the study area, their channel axes are buried behind the outcrop and therefore only the channel margins, which intersect the NW-SE oriented outcrop belt are exposed (Fig. 13). Their elongate geometry is an apparent effect of the outcrop orientation, highly oblique to the SE-directed paleoflow. The same interpretation of channel

margin deposits can be invoked for the elongated lenticular sandbodies observed towards N, in the upper part of CS2B (Fig. 13).

### 5.3.3. Isolated channels and channel complexes

**Description.** In the study area, the upper portion of the GF formation is characterized by the widespread occurrence of isolated elementary channels and channel complexes (Fig. 10). Directly above CS2, these isolated sedimentary bodies are initially embedded within, and deeply incisional into, F.A.2 sand-prone deposits and then, higher in the stratigraphy, into a nearly 700 m thick succession of F.A.3 mud-prone deposits (Figs. 4, 13). Isolated channel elements are commonly filled by amalgamated LF2B sandstones and capped by multiple sets of LF4 cross-stratified sandstones. Abundant extra-formational LF1A conglomerates and LF1B mudclast-rich conglomerates mantle prominent concave-upward, basal erosion surfaces and subordinate internal surfaces that define a well-developed multistorey architecture (Fig. 9B). Isolated channel elements range in thickness from 13 to 26 m and show average widths of ~350 m, but ranging from 180 m to 450 m (e.g., Pitts et al., 2017; Table 2). Basal paleocurrent indicators reveal a main current flow directed toward S-SE ( $151^\circ$ ), ranging from  $106^\circ$  to  $194^\circ$  (Fig. 5).

**Interpretation.** Isolated channel elements and channel complexes in the upper part of the GF succession have been interpreted by previous workers as large submarine slump deposits (Pescatore et al, 1980; Loiacono, 1993), produced by catastrophic avalanche processes induced by seismic shocks (Boiano, 1997; Giannandrea et al., 2016). However, the marked erosional character, the concave-up geometry of the sharp bases and the systematic internal facies distribution of these very coarse-grained sandbodies indicate deposition in submarine channels from multiple sediment gravity flows. Their dimensions, stratigraphic architectures and the abundance of LF1A conglomerates and poorly-sorted LF2B sandstones suggest that these sandbodies can be interpreted as low-sinuosity, incisional elementary channels.

As mentioned above, the thick F.A.3 mud-prone succession encasing the isolated channels (Fig. 13) can be interpreted to represent background slope deposits resulting from unfocussed, ramp-sourced turbidity currents (e.g., Figueiredo et al., 2010). Their deposition is possibly related to the general shift of the deep-water system along the depositional profile (see below in the discussion).

### 5.4. Channel planforms and stacking pattern

The spectacular exposures of the GF formation throughout the outcrop belt (Fig. 2) offer an excellent opportunity for the reconstruction of the stratigraphic relationships between the main architectural units at the scale of the deep-water system. In particular, these outcrops allow the analysis of the stacking pattern characterizing the channelized units, a crucial element to decipher the complex evolution of the GF formation in the study area and the role played by its main driving factors.

Submarine channel-belt architectures are typically dominated by the vertical aggradation of the channel-fill deposits, which record channel migration and document repeated phases of infill and incision (e.g., Sylvester et al., 2011; Hodgson et al., 2011; Jobe et al., 2016). Stacking patterns dominated by vertical aggradation are usually developed in highly-confined channel systems with high rates of deposition (e.g., Labourdette and Bez, 2010; Janocko et al., 2013; Macauley and Hubbard, 2013) and the GF formation represents an excellent example of such systems.

The stacking architectures of the channelized units preserved in the GF formation have been analyzed through the reconstruction of the channels' planform geometries (Fig. 14A). Major shifts in intra-element position (e.g., margin, off-axis or axis) were inferred from the channel-fill deposits within CS2 and the uppermost isolated channels/channel complexes, which are the best exposed units in the study area. The architectural data have been mapped and combined with paleoflow measurements from channel-fill deposits and heterolithic "out-of-channel" packages (Fig. 5), allowing the progressive plan view reconstruction of the stacked channel deposits (Fig. 14A). Within CS2, six "time slices" have been considered to describe the variability of the large-scale planform geometries (Fig. 14A). These distinct stages in CS2 evolution roughly correspond to the major extensive erosion surfaces identified at the base of CS2A and within CS2B, which separate discrete channel complexes. Due to the oblique outcrop belt orientation relative to paleoflow, the margins of individual channel complexes are not always exposed and direct measurements of their widths are difficult. To obtain a reliable estimation of channel-complex widths, the above-mentioned field observations have been compared with similar submarine channel-complex features from literature, compiled from many analogous channel systems (e.g., Campion et al., 2005; Thomas and Bodin, 2013; Stright et al., 2014). Accordingly, a constant channel-complex down-dip width of nearly 1000 m was assumed to reconstruct channel-complex architectures, based on their average maximum thickness measurements from outcrop (~ 75 m). The resulting planform channel patterns show an overall low degree of sinuosity along the 13-km long outcrop belt. Furthermore, two additional time slices describe the planforms of isolated channels and channel complexes in the upper part of the GF succession, which exhibit a slightly higher degree of sinuosity than CS2 channel complexes, albeit maintaining a relatively straight geometry (Fig. 14A).

Plan view reconstructions are used to project the inferred stacking trajectories of the GF channelized units in three-dimensions. A nearly E-W oriented sketch cross-section, cutting the GF channels roughly perpendicular to the regional paleoflow direction, provides a representation of the general migration pattern across that specific transect and allows the stacking behavior of the channelized units to be analyzed (Fig. 14B). At the scale of the channel system, CS2 exhibits a marked aggradational architecture, revealed by the limited lateral offset of its stacking channel complexes. This stacking pattern indicates that the channelized units migrate laterally, but at lower rates compared to the aggradation rate of the whole system. On the assumption that the inferred scale of lateral channel movement is correct, it can be inferred that the composite stacking pattern of CS2

results from the limited lateral migration of the channel system back and forth across the basin axis, initially directed towards W-SW and then back towards E-NE (Fig. 14B). This “zig-zag” migration pattern is recorded in the variable nature of the overbank deposits exposed between channel belts CS2A and CS2B, characterizing the central portion of the GF succession in the study area (Fig. 4). This extensive heterolithic package reaches a maximum thickness of approximately 400 m, pinching-out towards the north, where CS2A and CS2B converge (Fig. 4). At the large scale, a clear fining-then coarsening-upward trend has been documented. This composite stratigraphic trend is interpreted to be related to the coupled lateral migration and aggradation through time of the channelized depocenter of CS2 (e.g., Schwarz and Arnott, 2007; Hubbard et al., 2009). Specifically, the large-scale fining-upward trend within the lower part of the heterolithic succession (i.e., from F.A.2 proximal overbank deposits above CS2A to F.A.3 distal overbank deposits) coincides with the combined aggradation and migration of the active part of CS2 towards the W-SW, away from the site of deposition of the overbank package. Conversely, the subsequent large-scale coarsening-upward trend in the upper part of the overbank succession (i.e., from distal F.A.3 to proximal F.A.2 deposits occurring directly beneath CS2B) is interpreted to reflect the coupled aggradation and migration of CS2 back to the E-NE.

## 6. DISCUSSION

### 6.1. General architecture of the Gorgoglione Flysch system

Channel complexes and complex sets forming prominent deep-water systems are commonly imaged in seismic reflection datasets acquired by the hydrocarbon industry. These systems dominantly show a composite stratigraphic architecture consisting of broad, laterally-stacked channel complex and complex-set fills at the base, followed by nearly vertically-aligned and aggradational channel complexes and complex-sets at the top (Sylvester et al., 2011; Jobe et al., 2016). This typical sequence of channel architectural styles records a multi-phase degradational-aggradational trend that has been documented globally in both seismic (e.g., Deptuck et al., 2003; Janocko et al., 2013, Covault et al., 2016) and outcrop (e.g., Brunt et al., 2013a; Hodgson et al., 2011; Macauley and Hubbard, 2013) datasets.

While typically imaged in seismic datasets (e.g., Deptuck et al., 2003) and efficiently predicted by 3D surface-based stratigraphic forward models (e.g., Sylvester et al., 2011), the early-stage laterally-offset channels and channel complexes are difficult to recognize in outcrop and have been documented only in few cases (e.g., Di Celma et al., 2011; Bain and Hubbard, 2016). Early-stage, high-mobility channels show limited vertical aggradation and are commonly erosional and bypass-dominated, cannibalizing their own deposits as they migrate laterally (Deptuck et al., 2003; Covault et al., 2016). As a result, there is a limited preservation of the channel fills towards the base of the channel systems (Hodgson et al., 2011), with discontinuous remnants of sandy channels and

relatively thick packages of thinly bedded, mud-prone overbank deposits overlaying the broad basal erosion surface (Deptuck et al., 2003; McHargue et al., 2011). Due to their heterolithic and mud-rich nature, outcrop exposures of these basal overbank deposits may not be well preserved, being often weathered or covered by vegetation.

In the GF succession, these broad, laterally offset-stacked channel complexes and complex-sets comprising the lower portion of deep-water systems observed elsewhere have not been recognized. It is unclear if they are lacking or if this is due to limited outcrop or to the highly oblique orientation of the outcrop belt. The entire CS2 is instead characterized by a prominent aggradational nature combined with a limited lateral offset of its component channel complexes (Fig. 14B), resulting in a stacking pattern typically attributed to the late stages of channel complex-sets evolution (e.g., Myall et al., 2006; Bain and Hubbard, 2016).

## 6.2. Effects of thrust tectonics on CS2 stacking pattern

Relationships between thrust tectonics and the sedimentary record in foreland basin systems have been investigated mainly at regional scale (Roure, 2008 and references therein). However, reliable models predicting the architectural evolution of thrust-related depositional sequences are still poorly developed. The Apennine mountain chain developed in response to W-dipping subduction, where thrust-related folds were transported down into the subduction zone while they were forming (Doglioni, 1993). This process is thought to have induced high rates of regional subsidence in the foredeep (up to 1600 m/M.y.) due to the fast eastward rollback of the hinge of the W-dipping subduction zone (i.e., flexural subsidence; Mariotti and Doglioni, 2000). As a consequence of the prominent creation of accommodation space, a substantial portion of the foreland basin filling developed onto the active accretionary wedge (i.e., within the wedge-top basin, sensu DeCelles and Giles, 1996), favouring the development of thrust-top depozones (Fig. 15).

Significant changes in the accommodation space within the Plio-Pleistocene wedge-top basin of the Southern Apennines were mostly attributed to flexural subsidence in combination with thrust activity (Patacca and Scandone 2004). This tectonic mechanism can be assumed to be valid for the entire evolution of the Apennines (Doglioni and Prosser, 1997), including during Miocene times. The stratigraphic characters of the depositional sequences developed within the Apennine wedge-top basin are closely controlled by the trajectories of the thrusts that were active during sedimentation (Patacca and Scandone 2007). The active thrusts in the Apennine thrust-and-fold belt primarily propagate following one of two main trajectories (Fig. 15): (i) an inner trajectory, across the base of the exposed chain (i.e., out-of-sequence thrust); or (ii) an outer trajectory, which moves the front of the accretionary wedge (i.e., in-sequence thrust; Patacca and Scandone, 2007). Thrusts activate alternatively along these trajectories, which represent the inner and the outer margins of the wedge-top basin, respectively (Fig. 15). Accordingly, sedimentary successions evolving in wedge-top

depozones should record the interplay between the flexural subsidence and the growth of the active thrust. As a result, the maximum increase of the accommodation space takes place during periods of out-of-sequence thrust propagation, when flexural subsidence is predominant in the basin (Patacca and Scandone, 2001).

Internal channel stacking architecture of the GF system can be interpreted to be governed by either autogenic or allogenic processes. Significant creation of accommodation space promotes the development of marked aggradational architectures in submarine channel systems (e.g., Clark and Cartwright, 2011; Hodgson et al., 2011), as documented in CS2. Various mechanisms have been proposed to explain the migration trajectories commonly observed in submarine channel systems, including turbidity current flow properties (Kolla et al., 2007; Janocko et al., 2013), progressive levee growth (Peakall et al., 2000; Jobe et al., 2016), sediment supply versus accommodation (Kneller, 2003), changes in equilibrium profile (Hodgson et al., 2011) and effects of basin tectonics (Clark and Cartwright, 2009). However, the trigger for lateral channel migration is still poorly understood and many studies invoke complex interactions between these autogenic and allogenic processes (e.g., Hubbard et al., 2009; Di Celma et al., 2011; Thomas and Bodin, 2013). Among the different mechanisms that can be invoked, the activity of the thrusts that configured a narrow turbidite basin might have played an important role in controlling the migration trajectories of the stacked channelized units in CS2. As mentioned above, the GF system evolved during the Miocene, concurrently with the early growth of the Southern Apennine orogen. Accordingly, it is likely that the high rates of tectonic activity in the thrust-and-fold belt (Patacca and Scandone 2007) affected the development of the GF system. Thrust-faults in the Apennine accretionary wedge typically show a slip rate variability on a timescale up to 500 K.y. (Gunderson et al., 2013), consistent with the time span during which CS2 evolved, according to biostratigraphic data reported by Giannandrea et al. (2016). In this scenario, the reconstructed migration pattern of CS2 might have been influenced by the variable rate of growth of the internal, out-of-sequence thrust, which competed during its development with the ongoing subsidence of the basin (Fig. 16). The subsidence was associated with the progressive flexure of the underlying plate in the subduction zone and is assumed to have developed at constant rates during the evolution of the deep-water system. When the growth rate of the internal thrust was lower than the regional subsidence rate, the fast eastward roll-back in the subduction zone tilted the basin towards SW and likely determined the initial migration of CS2 channel thalweg towards W-SW (Fig. 16A). Conversely, when the thrust growth rate outpaced the regional subsidence rate, the channel system depocenter was progressively shifted towards E-NE, away from the axis of uplift of the thrust (Fig. 16B), in a process referred to as “deflection” (Clark and Cartwright, 2009; 2011).

It is worth noting that the maximum lateral offset displayed by the major channelized units in CS2 is less than one kilometer (Fig. 14B), relatively limited if compared to the stacking patterns typically documented in other submarine channel systems worldwide (e.g., Hubbard et al., 2009; Sylvester et

al., 2011; Bain and Hubbard, 2016). On the assumption that the scale of lateral migration is correct, a possible interpretation for this limited lateral offset might be that it is an effect of the tectonically-induced narrow basin configuration. In general, a significant structural confinement imparted by the basin physiography tends to limit the ability of a channel system to migrate laterally, resulting in a restricted lateral stacking variability of the component channelized units, and thus preventing the large-scale avulsion of the channel belt (Hubbard et al., 2009; Labourdette and Bez, 2010). Accordingly, the reduced lateral space available within the narrow GF basin might have limited the lateral migration of the stacked channel complexes that form CS2 (Fig. 14B) and prevented the avulsion of the channel system to new positions.

### 6.3. Stratigraphic evolution of the GF deep-water system

The reconstruction of the evolutionary history of an ancient turbidite system is one of the main goals of recent outcrop studies (e.g., Pickering et al., 2015; Di Celma et al., 2016; Greene and Surpless, 2017). For this purpose, the accurate interpretation of the stratigraphic record and the analysis of spatial and temporal changes in depositional architectures are of primary importance (e.g., Mutti and Normark, 1987; Romans et al., 2011; Jobe et al., 2016). The nearly 2 km thick GF succession presented in this study records the complex interplay between the depositional processes controlling sand accumulation (i.e., weakly-confined channel fills vs incisional channel fills) and the driving factors that presumably governed the aggradation and stacking pattern of the deep-water channels (i.e., increasing subsidence, syn-sedimentary thrust tectonics and structural basin confinement). At the scale of the deep-water system, the observed juxtaposition of different channel architectures and heterolithic deposits is interpreted to have been governed by the alternate in- and out-of-sequence tectonic pulses of the basin-bounding thrusts, which controlled the coarse clastic inputs sourced from the orogenic hinterland. This overall change in depositional style likely reflects a varying position of the GF system along the paleo-depositional profile.

In submarine channel systems, a key control on flow properties and resulting architectural geometries of channel fills is commonly attributed to the submarine slope gradient (e.g., Wynn et al., 2002; Kneller, 2003), which may be modified by multiple factors, such as faulting, diapirism, sediment accretion, differential compaction, mass wasting (Prather, 2000) or tectonic tilting (McCaffrey et al., 2002; Ferry et al., 2005). Continued erosion or deposition may modify the slope profile, in relation to externally driven changes in volumes and frequencies of gravity flows (Cronin et al., 2000; Kneller, 2003).

The depositional and architectural features of the amalgamated incisional channels of CS1 are commonly associated with slope channel-fill deposits (e.g., Hubbard et al., 2014; Pemberton et al., 2016). This might suggest a likely initiation and development for these channels in a slope environment (e.g., Figueiredo et al., 2013; Bayliss and Pickering, 2015a), which presumably

characterized the earlier phases of the GF basin evolution (Fig. 17A). The abundance of extraformational conglomerates (LF1A) reflects the protracted denudation of the source area, located to the W-NW in the orogenic hinterland (Critelli and Loiacono, 1988; Critelli et al., 2017). High-energy sediment-gravity flows likely developed in response to increased gradients in the staging area, determined by the activity of the internal thrust structures of the Apennine thrust-and-fold belt, which progressively uplifted the chain and promoted its erosion (Fig. 17A). A gradual deactivation of the coarse clastic inputs from the sediment source area, possibly related to the decreasing rates of tectonic uplift in the SW and the concomitant early activation of the outer thrust to the NE, resulted in the deposition of the ~100 m thick interval of F.A.3 mud-prone heterolithic deposits overlying CS1 (Figs. 4, 17B). This interval was also tilted toward SW as a result of the north-eastern thrust growth (Fig. 17B). According to Giannandrea et al. (2016), the outer thrust developed at the Burdigalian-Langhian transition and marked the north-eastern boundary of the GF basin, which started to be configured as a narrow and NW-SE elongated thrust-top basin with a south-eastward dipping basin floor. The thick package of F.A.3 mud-prone deposits might have recorded a retrogradation of the slope environment and a substantial reduction of the seafloor gradient, favoring the establishment of a near base-of-slope setting. A similar stratigraphic trend, related to tectonically-induced variations of the seafloor gradient, has been documented by Bayliss and Pickering (2015b) in the Morillo System of the Ainsa basin (Spain).

After the initial phase of slope gradient readjustment, erosion and deposition of CS2 took place, prompted by the re-activation of the internal, out-of-sequence regional thrust that restored the coarse clastic inputs to the basin from the western source area (Fig. 17C). This large channel complex-set comprises amalgamated, high-aspect-ratio, weakly-confined channel elements, flanked by sand-prone overbank deposits (F.A.2). These particular types of channel architectures have been commonly documented in areas of low to moderate gradient on a paleo-depositional profile, in lower slope or base-of-slope settings, associated with strikingly sand-rich overbank deposits (e.g., Maier et al., 2011; Brunt et al., 2013b; Pemberton et al., 2016).

Higher up in the stratigraphy, amalgamated weakly-confined channels gradually evolve into isolated, low-aspect-ratio incisional channels, deeply incisional into the surrounding mudstones and very thin-bedded sandstones of F.A.3, interpreted as slope deposits (Fig. 17D). Evidence of protracted bypass of energetic gravity flows that commonly cut down for tens of meters into very fine-grained slope deposits are generally associated with middle- to upper-slope channels, commonly recognized in outcrops (e.g., Gardner et al., 2003; Hubbard et al., 2014) and seismic datasets (e.g., Mayall et al., 2006; Jobe et al., 2015).

In summary, the stratigraphic trend documented through the middle and upper portions of the GF succession, starting from the deposition of CS2, records a progressive increase of the slope gradient that resulted in incremental increases in confinement of turbidity currents through time, as indicated

by the stratigraphic transition from high-aspect-ratio to low-aspect-ratio channels (Prather, 2003; Pemberton et al., 2016). The increase of the slope-gradient is also marked by a progressive variation in the nature of the out-of-channel, heterolithic deposits upward in the stratigraphy, from sand-prone (F.A.2) to mud-prone (F.A.3). The overall upward change in sand content and channel architectural style is therefore interpreted to represent the progradation of a slope channel system (i.e., upper part of the GF succession) over a base-of-slope, weakly confined sand-prone channel system (i.e., CS2). This marked progradational trend developed during the late Miocene in association with the progressive infill of the narrow primary confinement (Fig. 17). A comparable stratigraphic trend has been documented in the Unit B of the Laingsburg Formation in the Karoo Basin of South Africa (Flint et al., 2011; Brunt et al., 2013b), where the stratigraphic change in channel architectural style has been interpreted to record the overall progradation of the turbidite system.

## 7. CONCLUSIONS

The deep-water strata of the Gorgoglione Flysch Formation document a protracted history of sediment transfer and deposition through a long-lived channel system, developed during the late Miocene in a narrow and elongated thrust-top basin of the Southern Apennines (Italy). A wide range of erosional and depositional processes are recorded in an exceptionally-preserved outcrop belt, oriented sub-parallel to the basin axis and regional paleoflow. The spectacular exposures of the Gorgoglione Flysch succession provide an excellent opportunity to characterize the spatio-temporal evolution of a submarine channel system at a scale similar to that commonly imaged on seismic datasets, but with the stratigraphic detail exclusive of outcrop studies.

Channel-fill facies, including matrix-supported extraformational conglomerates, mudclast-rich conglomerates and coarse-grained sandstones, are laterally juxtaposed against sand-prone and mud-prone, out-of-channel heterolithic deposits. Across the study area, the stratigraphic distribution and variability of channel architecture of the Gorgoglione Flysch succession strongly controls the seismic-scale depositional style of the main architectural units and their depositional character. From the base of the succession, two discrete channel complex-sets have been recognized, separated by an approximately 100 m thick package of heterolithic slope deposits: (1) CS1, which is isolated in the lowermost portion of the Gorgoglione Flysch succession and is composed of amalgamated, low aspect ratio, incisional channels; and (2) CS2, which is exposed extensively throughout the study area and represents nearly the 80% of the preserved channel fill sandstones. This prominent channel complex-set comprises amalgamated, high aspect ratio, weakly-confined channels flanked by heterolithic overbank deposits and exhibits a markedly aggradational stacking pattern with a limited lateral offset of its component channel complexes. Above CS2, isolated channels and channel complexes occur, consisting of incisional elementary channels embedded within, and considerably incisional into, mud-prone slope deposits.

The observed sequence of channelized architectural units is interpreted to have been governed at multiple scales by the thrust tectonics of the Southern Apennines, in combination with a high subsidence rate that promoted significant aggradation. The alternate in- and out-of-sequence tectonic pulses of the thrust structures delimiting the Gorgoglione Flysch basin might have controlled the activation of the coarse-clastic inputs and the resulting stacking architectures of the channelized units. The tectonic confinement resulted in a narrow basin morphology and possibly limited the lateral offset in channel stacking documented in CS2, preventing large-scale avulsions.

The overall change in depositional style, revealed by the marked juxtaposition of different channel architectures and heterolithic deposits, allowed the temporal and spatial evolution of the Gorgoglione Flysch system to be reconstructed. The general stratigraphic trend likely reflects a varying position of the Gorgoglione Flysch deep-water system along the paleo-depositional profile. In particular, the upward change in sand content and channel architectures, expressed in the gradual stratigraphic transition from CS2 to the upper isolated channels, is interpreted to record the general progradation of a slope channel system over a near base-of-slope channel system.

In conclusion, examination of the Gorgoglione Flysch succession highlights the key architectural and sedimentological features typical of channel systems developed within confined and elongate basins, supporting the development of a well-constrained predictive model for sediment distribution that can be translated to analogous depositional systems in the subsurface. The comprehensive dataset presented from the northern sector of the GF basin represents a rare case study from outcrop of depositional and erosional processes in a confined base-of-slope to slope setting. The results of this study should find wide applicability in other basins, particularly those that formed in active tectonic settings. The documented depositional styles, scale of the component architectural units, and stacking patterns of the sandbodies provide useful comparisons with submarine channel systems where important tectonic structures have controlled the sedimentation.

## **ACKNOWLEDGMENTS**

The people of Pietrapertosa and Castelmezzano are greatly acknowledged for their kindness and support after tiring days of fieldwork. Funding for this project was provided by University of Camerino and Turbidites Research Group industry sponsors: BP, Conoco Phillips, ENI, Hess, Murphy, OMV, Shell and Statoil. C.I.C. greatly thanks Alan Pitts and Fabio Lunerti for their capable assistance in the field. Rufus Brunt, Neal Auchter and the Associate Editor Ian Kane are gratefully acknowledged for their constructive comments and thoughtful reviews, which helped to improve an earlier version of the manuscript and sharpened the focus of this paper.

1 **REFERENCES**

- 2 **Allen, J.R.** (1963) The classification of cross-stratified units with notes on their origin. *Sedimentology*, **2**(2),  
3 93-114.
- 4 **Alpak, F.O., Barton, M.D. and Naruk, S.J.** (2013) The impact of fine-scale turbidite channel architecture on  
5 deep-water reservoir performance. *AAPG Bulletin*, **97**(2), 251-284.
- 6 **Arnott, R.W.C., Navarro, L. and Khan, Z.A.** (2011) Contrasting the stratal architecture of highly-confined and  
7 poorly-confined deep-marine sinuous channel systems – an outcrop perspective. In: *Internal*  
8 *architecture, bedforms and geometry of turbidite channels* (Eds. Mayall, M., Kane, I., McCaffrey,  
9 W.D.), The geological Society of London, June 20-21, 2011.
- 10 **Babonneau, N., Savoye, B., Cremer, M. and Bez, M.** (2010) Sedimentary architecture in meanders of a  
11 submarine channel: detailed study of the present Congo turbidite channel (Zaiango project). *Journal*  
12 *of Sedimentary Research*, **80**(10), 852-866.
- 13 **Bain, H.A. and Hubbard, S.M.** (2016) Stratigraphic evolution of a long-lived submarine channel system in the  
14 Late Cretaceous Nanaimo Group, British Columbia, Canada. *Sedimentary Geology*, **337**, 113-132.
- 15 **Barton, M., O'Byrne, C., Pirmez, C., Prather, B., Van der Vlugt, F., Alpak, F.O. and Sylvester, Z.** (2010)  
16 Turbidite channel architecture: Recognizing and quantifying the distribution of channel-base drapes  
17 using core and dipmeter data. In: *Dipmeter and Borehole Image Log Technology* (Eds. Pöppelreiter,  
18 M., García-Carballido, C., Kraaijeveld, M.A.), AAPG Memoir, 92, 195–210.
- 19 **Bayliss, N.J. and Pickering, K.T.** (2015 a) Transition from deep-marine lower-slope erosional channels to  
20 proximal basin-floor stacked channel–levée–overbank deposits, and syn-sedimentary growth  
21 structures, Middle Eocene Banastón System, Ainsa Basin, Spanish Pyrenees. *Earth-Science*  
22 *Reviews*, **144**, 23-46.
- 23 **Bayliss, N.J. and Pickering, K.T.** (2015 b) Deep-marine structurally confined channelized sandy fans: Middle  
24 Eocene Morillo System, Ainsa Basin, Spanish Pyrenees. *Earth-Science Reviews*, **144**, 82-106.
- 25 **Beaubouef, R.T.** (2004) Deep-water leveed-channel complexes of the Cerro Toro Formation, Upper  
26 Cretaceous, southern Chile. *AAPG Bulletin*, **88**(11), 1471-1500.
- 27 **Beaubouef, R.T., Rossen, C., Zelt, F.B., Sullivan, M.D., Mohrig, D.C. and Jennette, D.C.** (1999) Deep-  
28 water sandstones, Brushy Canyon Formation, west Texas. Field guide for American Association of  
29 Petroleum Geologists, Hedberg Field Research Conference. AAPG Continuing Education Course  
30 Note Series 40, p. 47.
- 31 **Boiano, U.** (1997) Anatomy of a siliciclastic turbidite basin: the Gorgoglione Flysch, Upper Miocene, southern  
32 Italy: physical stratigraphy, sedimentology and sequence-stratigraphic framework. *Sedimentary*  
33 *Geology*, **107**(3), 231-262.
- 34 **Bouma, A.H.** (1962) *Sedimentology of Some Flysch Deposits; A Graphic Approach to Facies Interpretation:*  
35 Amsterdam, Elsevier, 168 pp.
- 36 **Brunt, R.L. and McCaffrey, W.D.** (2007) Heterogeneity of fill within an incised channel: The Oligocene Gres  
37 du Champsaur, SE France. *Marine and Petroleum Geology*, **24**(6), 529-539.

- 38 **Brunt, R.L., Di Celma, C.N., Hodgson, D.M., Flint, S.S., Kavanagh, J.P. and van der Merwe, W.C.** (2013  
39 a) Driving a channel through a levee when the levee is high: An outcrop example of submarine down-  
40 dip entrenchment. *Marine and Petroleum Geology*, **41**, 134-145.
- 41 **Brunt, R.L., Hodgson, D.M., Flint, S.S., Pringle, J.K., Di Celma, C., Pr lat, A. and Grecula, M.** (2013 b)  
42 Confined to unconfined: anatomy of a base of slope succession, Karoo Basin, South Africa. *Marine*  
43 *and Petroleum Geology*, **41**, 206-221.
- 44 **Butler, R.W. and Tavarnelli, E.** (2006) The structure and kinematics of substrate entrainment into high-  
45 concentration sandy turbidites: a field example from the Gorgoglione 'flysch' of southern Italy.  
46 *Sedimentology*, **53**(3), 655-670.
- 47 **Camacho, H., Busby, C.J. and Kneller, B.** (2002) A new depositional model for the classical turbidite locality  
48 at San Clemente State Beach, California. *AAPG Bulletin*, **86**(9), 1543-1560.
- 49 **Campion, K.M., Sprague, A.R. and Sullivan, M.D.** (2005) Architecture and lithofacies of the Capistrano  
50 Formation (Miocene-Pliocene), San Clemente, California. *SEPM, Pacific Section, Guide Book 100*, 42  
51 pp.
- 52 **Cavalcante, F., Prosser, G., Agosta, F., Belviso, C. and Corrado, G.** (2015) Post-depositional history of the  
53 Miocene Gorgoglione Formation (southern Apennines, Italy): inferences from mineralogical and  
54 structural analyzes. *Bull. Soc. G ol. Fr.* **186**(4-5), 243-256.
- 55 **Clark, I.R. and Cartwright, J.A.** (2009) Interactions between submarine channel systems and deformation in  
56 deep-water fold belts: Examples from the Levant Basin, Eastern Mediterranean Sea. ***Marine and***  
57 ***Petroleum Geology***, **26**(8), 1465-1482.
- 58 **Clark, I.R. and Cartwright, J.A.** (2011) Key controls on submarine channel development in structurally active  
59 settings. *Marine and Petroleum Geology*, **28**(7), 1333-1349.
- 60 **Clark, J.D. and Pickering, K.T.** (1996) Architectural elements and growth patterns of submarine channels:  
61 application to hydrocarbon exploration. *AAPG Bulletin*, **80**(2), 194-220.
- 62 **Covault, J.A., Sylvester, Z., Hubbard, S.M., Jobe, Z.R. and Sech, R.P.** (2016). The stratigraphic record of  
63 submarine – channel evolution. *The Sedimentary Record*, **14**, 4-11.
- 64 **Critelli, S. and Loiacono, F.** (1988) Provenienza e dispersione dei sedimenti nel flysch di Gorgoglione  
65 (Langhiano–Tortoniano, Appennino Lucano): Implicazioni sull'evoluzione delle mode detritiche  
66 arenacee nell'orogene sudappenninico. *Mem. Soc. Geol. It.*, **41**, 809-826.
- 67 **Critelli, S., Muto, F., Perri, F. and Tripodi, V.** (2017) Interpreting provenance relations from sandstone detrital  
68 modes, southern Italy foreland region: Stratigraphic record of the Miocene tectonic evolution. *Marine*  
69 *and Petroleum Geology*.
- 70 **Cronin, B.T., Hartley, A.J., Celik, H., Hurst, A., Turkmen, I. and Kerey, E.** (2000) Equilibrium profile  
71 development in graded deep-water slopes: Eocene, Eastern Turkey. *Journal of the Geological Society*,  
72 **157**(5), 943-955.
- 73 **Cullis, S., Colombrera, L., Patacci, M. and McCaffrey, W.D.** (2018) Hierarchical classifications of the  
74 sedimentary architecture of deep-marine depositional systems. *Earth-Science Reviews*, **179**, 38-71

- 75 **DeCelles, P.G. and Giles, K.A.** (1996) Foreland basin systems. *Basin research*, **8**(2), 105-123.
- 76 **Deptuck, M.E., Steffens, G.S., Barton, M. and Pirmez, C.** (2003) Architecture and evolution of upper fan  
77 channel-belts on the Niger Delta slope and in the Arabian Sea. ***Marine and Petroleum Geology***,  
78 **20**(6), 649-676.
- 79 **Di Celma, C.** (2011) Sedimentology, architecture, and depositional evolution of a coarse-grained submarine  
80 canyon fill from the Gelasian (early Pleistocene) of the Peri-Adriatic basin, Offida, central Italy.  
81 *Sedimentary Geology*, **238**, 233-253.
- 82 **Di Celma, C.N., Brunt, R.L., Hodgson, D.M., Flint, S.S. and Kavanagh, J.P.** (2011) Spatial and temporal  
83 evolution of a Permian submarine slope channel–levee system, Karoo Basin, South Africa. *Journal of*  
84 *Sedimentary Research*, **81**(8), 579-599.
- 85 **Di Celma, C., Cantalamessa, G. and Didaskalou, P.** (2013) Stratigraphic organization and predictability of  
86 mixed coarse-grained and fine-grained successions in an upper slope Pleistocene turbidite system of  
87 the Peri-Adriatic basin. *Sedimentology*, **60**(3), 763-799.
- 88 **Di Celma, C., Teloni, R. and Rustichelli, A.** (2016) Evolution of the Gelasian (Pleistocene) slope turbidite  
89 systems of southern Marche (Peri-Adriatic basin, central Italy). *Journal of Maps*, **12**(1), 137-151.
- 90 **Dogliani, C.** (1993) Some remarks on the origin of foredeeps. *Tectonophysics*, **228**(1-2), 1-20.
- 91 **Dogliani, C. and Prosser, G.** (1997) Fold uplift versus regional subsidence and sedimentation rate. *Marine*  
92 *and Petroleum Geology*, **14**(2), 179-190.
- 93 **Eschard, R., Albouy, E., Deschamps, R., Euzen, T. and Ayub, A.** (2003) Downstream evolution of turbidite  
94 channel complexes in the Pab Range outcrops (Maastrichtian, Pakistan). *Marine and Petroleum*  
95 *Geology*, **20**, 691–710.
- 96 **Etienne, S., Mulder, T., Bez, M., Desaubliaux, G., Kwasniewski, A., Parize, O., Dujoncquoy, E. and Salles,**  
97 **T.** (2012) Multiple scale characterization of sand-rich distal lobe deposit variability: examples from the  
98 Annot Sandstones Formation, Eocene–Oligocene, SE France. *Sedimentary Geology*, **273**, 1-18.
- 99 **Ferry, J.N., Mulder, T., Parize, O. and Raillard, S.** (2005) Concept of equilibrium profile in deep-water turbidite  
100 system: effects of local physiographic changes on the nature of sedimentary process and the  
101 geometries of deposits. *Geol. Soc. London Spec. Publ.*, **244**(1), 181-193.
- 102 **Figueiredo, J.J., Hodgson, D.M., Flint, S.S. and Kavanagh, J.P.** (2010) Depositional environments and  
103 sequence stratigraphy of an exhumed Permian mudstone-dominated submarine slope succession,  
104 Karoo Basin, South Africa. *Journal of Sedimentary Research*, **80**(1), 97-118.
- 105 **Figueiredo, J.J., Hodgson, D.M., Flint, S.S. and Kavanagh, J.P.** (2013) Architecture of a channel complex  
106 formed and filled during long-term degradation and entrenchment on the upper submarine slope, Unit  
107 F, Fort Brown Fm., SW Karoo Basin, South Africa. *Marine and Petroleum Geology*, **41**, 104-116.
- 108 **Fildani, A., Hubbard, S.M., Covault, J.A., Maier, K.L., Romans, B.W., Traer, M. and Rowland, J.C.** (2013)  
109 Erosion at inception of deep-sea channels. *Marine and Petroleum Geology*, **41**, 48-61.
- 110 **Flint, S.A., Hodgson, D.M., Sprague, A.R., Brunt, R.L., Van der Merwe, W.C., Figueiredo, J., Prelat, A.,**  
111 **Box, D., Di Celma, C. and Kavanagh, J.P.** (2011) Depositional architecture and sequence

- 112 stratigraphy of the Karoo basin floor to shelf edge succession, Laingsburg depocenter, South Africa.  
113 Marine and Petroleum Geology, **28**(3), 658-674.
- 114 **Gardner, M.H. and Borer, J.M.** (2000) Submarine channel architecture along a slope to basin profile, Brushy  
115 Canyon Formation, west Texas. SEPM Spec. Publ., **68**, 195-214.
- 116 **Gardner, M.H., Borer, J.M., Melick, J.J., Mavilla, N., Dechesne, M. and Wagerle, R.N.** (2003) Stratigraphic  
117 process-response model for submarine channels and related features from studies of Permian Brushy  
118 Canyon outcrops, West Texas. Marine and Petroleum Geology, **20**(6), 757-787.
- 119 **Ghosh, B. and Lowe, D.R.** (1993) The architecture of deep-water channel complexes, Cretaceous Venado  
120 sandstone member, Sacramento Valley, California. In: Advances in the Sedimentary Geology of the  
121 Great Valley Group, Sacramento Valley, California (Eds S.A. Graham and D.R. Lowe), SEPM, Pacific  
122 Section, Guidebook 73, 51–65.
- 123 **Giannandrea, P., Loiacono, F., Maiorano, P., Lirer, F. and Puglisi, D.** (2016) Geological map of the eastern  
124 sector of the Gorgoglione Basin (southern Italy). Italian Journal of Geosciences, **135**(1), 120-141.
- 125 **Greene, T.J. and Surpless, K.D.** (2017) Facies architecture and provenance of a boulder-conglomerate  
126 submarine channel system, Panoche Formation, Great Valley Group: A forearc basin response to  
127 middle Cretaceous tectonism in the California convergent margin. Geosphere, **13**(3), 838-869.
- 128 **Grundvåg, S.A., Johannessen, E.P., Helland-Hansen, W. and Plink-Björklund, P.** (2014) Depositional  
129 architecture and evolution of progradationally stacked lobe complexes in the Eocene Central Basin of  
130 Spitsbergen. Sedimentology, **61**(2), 535-569.
- 131 **Gueguen, E., Doglioni, C. and Fernandez, M.** (1998) On the post-25 Ma geodynamic evolution of the western  
132 Mediterranean. Tectonophysics, **298**(1), 259-269.
- 133 **Gunderson, K.L., Anastasio, D.J., Pazzaglia, F.J. and Picotti, V.** (2013) Fault slip rate variability on 10<sup>4</sup>–  
134 10<sup>5</sup> yr timescales for the Salsomaggiore blind thrust fault, Northern Apennines, Italy. Tectonophysics,  
135 **608**, 356-365.
- 136 **Hansen, L.A., Callow, R.H., Kane, I. A., Gamberi, F., Rovere, M., Cronin, B.T. and Kneller, B.C.** (2015)  
137 Genesis and character of thin-bedded turbidites associated with submarine channels. Marine and  
138 Petroleum Geology, **67**, 852-879.
- 139 **Hiscott, R.N., Hall, F.R. and Pirmez, C.** (1997) Turbidity-current overspill from the Amazon Channel: texture  
140 of the silt/sand load, paleoflow from anisotropy of magnetic susceptibility, and implications for flow  
141 processes. In: Proceedings - ocean drilling program scientific results, National Science Foundation,  
142 53-78.
- 143 **Hodgson, D.M., Di Celma, C.N., Brunt, R.L. and Flint, S.S.** (2011) Submarine slope degradation and  
144 aggradation and the stratigraphic evolution of channel–levee systems. Journal of the Geological  
145 Society, **168**(3), 625-628.
- 146 **Hubbard, S.M., de Ruig, M.J. and Graham, S.A.** (2009) Confined channel-levee complex development in an  
147 elongate depo-center: deep-water Tertiary strata of the Austrian Molasse basin. Marine and Petroleum  
148 Geology, **26**(1), 85-112.

- 149 **Hubbard, S.M., Covault, J.A., Fildani, A. and Romans, B.W.** (2014) Sediment transfer and deposition in  
150 slope channels: deciphering the record of enigmatic deep-sea processes from outcrop. Geological  
151 Society of America Bulletin, **126**(5-6), 857-871.
- 152 **Janocko, M., Nemeč, W., Henriksen, S. and Warchoř, M.** (2013) The diversity of deep-water sinuous channel  
153 belts and slope valley-fill complexes. Marine and Petroleum Geology, **41**, 7-34.
- 154 **Jobe, Z.R., Howes, N.C. and Auchter, N.C.** (2016) Comparing submarine and fluvial channel kinematics:  
155 Implications for stratigraphic architecture. Geology, **44**(11), 931-934.
- 156 **Kane, I.A., Kneller, B.C., Dykstra, M., Kassem, A. and McCaffrey, W.D.** (2007) Anatomy of a submarine  
157 channel–levee: an example from Upper Cretaceous slope sediments, Rosario Formation, Baja  
158 California, Mexico. Marine and Petroleum Geology, **24**(6), 540-563.
- 159 **Kane, I.A., Dykstra, M.L., Kneller, B.C., Tremblay, S. and McCaffrey, W.D.** (2009) Architecture of a coarse-  
160 grained channel–levée system: the Rosario Formation, Baja California, Mexico. Sedimentology, **56**(7),  
161 2207-2234.
- 162 **Kane, I.A., Catterall, V., McCaffrey, W.D. and Martinsen, O.J.** (2010) Submarine channel response to  
163 intrabasinal tectonics: The influence of lateral tilt. AAPG bulletin, **94**(2), 189-219.
- 164 **Kane, I.A. and Hodgson, D.M.** (2011) Sedimentological criteria to differentiate submarine channel levee  
165 subenvironments: exhumed examples from the Rosario Fm. (Upper Cretaceous) of Baja California,  
166 Mexico, and the Fort Brown Fm.(Permian), Karoo basin, S. Africa. Marine and Petroleum Geology,  
167 **28**(3), 807-823.
- 168 **Kneller, B.** (2003) The influence of flow parameters on turbidite slope channel architecture. Marine and  
169 Petroleum Geology, **20**(6), 901-910.
- 170 **Kneller, B.C. and McCaffrey, W.D.** (2003) The interpretation of vertical sequences in turbidite beds: the  
171 influence of longitudinal flow structure. Journal of Sedimentary Research, **73**(5), 706-713.
- 172 **Kolla, V., Posamentier, H.W. and Wood, L.J.** (2007) Deep-water and fluvial sinuous channels—  
173 Characteristics, similarities and dissimilarities, and modes of formation. Marine and Petroleum  
174 Geology, **24**(6), 388-405.
- 175 **Labourdette, R. and Bez, M.** (2010) Element migration in turbidite systems: Random or systematic  
176 depositional processes? AAPG Bulletin, **94**(3), 345-368.
- 177 **Larue, D.K. and Provine, K.G.** (1988) Vacillatory turbidites, Barbados. Sedimentary Geology, **57**(3-4), 211-  
178 219.
- 179 **Li, P., Kneller, B.C., Hansen, L. and Kane, I.A.** (2016) The classical turbidite outcrop at San Clemente,  
180 California revisited: An example of sandy submarine channels with asymmetric facies architecture.  
181 Sedimentary Geology, **346**, 1-16.
- 182 **Li, P., Kneller, B., Thompson, P., Bozetti, G. and Santos, T.d.** (2018) Architectural and facies organization  
183 of slope channel fills: Upper Cretaceous Rosario Formation, Baja California, Mexico. Marine and  
184 Petroleum Geology, doi: 10.1016/j.marpetgeo.2017.11.026.

- 185 **Loiacono, F.** (1974) Osservazioni sulla direzione delle paleocorrenti nel Flysch di Gorgoglione (Lucania). Boll.  
186 Soc. Geol. Ital., **93**, 1127-1155.
- 187 **Loiacono, F.** (1993) Geometrie e caratteri deposizionali dei corpi arenacei nella successione stratigrafica del  
188 Flysch di Gorgoglione (Miocene sup., Appennino meridionale). Boll. Soc. Geol. Ital., **112**, 909-922.
- 189 **Lowe, D.R.** (1982) Sediment gravity flows: II. Depositional models with special reference to the deposits of  
190 high-density turbidity currents. *Journal of Sedimentary Petrology*, **52**, 279 – 297.
- 191 **Macauley, R.V. and Hubbard, S.M.** (2013) Slope channel sedimentary processes and stratigraphic stacking,  
192 Cretaceous Tres Pasos Formation slope system, Chilean Patagonia. *Marine and Petroleum Geology*,  
193 **41**, 146-162.
- 194 **Maffione, M., Speranza, F., Cascella, A., Longhitano, S.G., and Chiarella, D.** (2013) A~ 125 post-early  
195 Serravallian counterclockwise rotation of the Gorgoglione Formation (Southern Apennines, Italy): New  
196 constraints for the formation of the Calabrian Arc. *Tectonophysics*, **590**, 24-37.
- 197 **Maier, K.L., Fildani, A., Paull, C.K., Graham, S.A., McHargue, T.R., Caress, D.W. and McGann, M.** (2011)  
198 The elusive character of discontinuous deep-water channels: New insights from Lucia Chica channel  
199 system, offshore California. *Geology*, **39**(4), 327-330.
- 200 **Mariotti, G. and Doglioni, C.** (2000) The dip of the foreland monocline in the Alps and Apennines. *Earth and*  
201 *Planetary Science Letters*, **181**(1), 191-202.
- 202 **Mayall, M. and Stewart, I.** (2000) The architecture of turbidite slope channels. In: *Deep-Water Reservoirs of*  
203 *the World: SEPM, Gulf Coast Section, 20th Annual Research Conference* (Vol. 578, p. 586).
- 204 **Mayall, M., Jones, E. and Casey, M.** (2006) Turbidite channel reservoirs—Key elements in facies prediction  
205 and effective development. *Marine and Petroleum Geology*, **23**(8), 821-841.
- 206 **McCaffrey, W.D., Gupta, S. and Brunt, R.** (2002) Repeated cycles of submarine channel incision, infill and  
207 transition to sheet sandstone development in the Alpine Foreland Basin, SE France. *Sedimentology*,  
208 **49**(3), 623-635.
- 209 **McCaffrey, W.D. and Kneller, B.C.** (2004) Scale effects of non-uniformity on deposition from turbidity currents  
210 with reference to the Gres d'Annot of SE France. *Geol. Soc. London Spec. Publ.*, **221**(1), 301-310.
- 211 **McHargue, T., Pyrcz, M.J., Sullivan, M.D., Clark, J.D., Fildani, A., Romans, B.W., Covault, J.A., Levy, M.,**  
212 **Posamentier, H.W. and Drinkwater, N.J.** (2011) Architecture of turbidite channel systems on the  
213 continental slope: Patterns and predictions. *Marine and Petroleum Geology*, **28**(3), 728-743.
- 214 **Migeon, S., Mulder, T., Savoye, B. and Sage, F.** (2012) Hydrodynamic processes, velocity structure and  
215 stratification in natural turbidity currents: results inferred from field data in the Var Turbidite System.  
216 *Sedimentary Geology*, **245**, 48-62.
- 217 **Mutti, E.** (1992) Turbidite sandstones. Agip, Istituto di geologia, Università di Parma.
- 218 **Mutti, E. and Normark, W.R.** (1987) Comparing examples of modern and ancient turbidite systems: problems  
219 and concepts. In: *Marine Clastic Sedimentology* (Eds J.K. Leggett and G.G. Zuffa), Graham and  
220 Trotman, London, pp. 1-38.

- 221 **Navarro, L., Khan, Z. and Arnott R.W.C.** (2007) Depositional architecture and evolution of a deep-marine  
222 channel-levee complex: Isaac Formation (Windermere Supergroup), Southern Canadian Cordillera.  
223 In: Atlas of deep-water outcrops (Eds T.H. Nilsen, R.D. Shew, G.S. Steffens, and J.R.J. Studlick),  
224 AAPG Studies in Geology, 56, CD-ROM, 22 p.
- 225 **Patacca, E. and Scandone, P.** (2001) Late thrust propagation and sedimentary response in the thrust-belt—  
226 foredeep system of the Southern Apennines (Pliocene-Pleistocene). In: Anatomy of an orogen: the  
227 Apennines and Adjacent Mediterranean Basins (Eds G.B. Vai and I.P. Martini), Kluwer Academic  
228 Publishers, Dordrecht, The Netherlands, 401-440.
- 229 **Patacca, E. and Scandone, P.** (2004) The Plio-Pleistocene thrust belt-foredeep system in the southern  
230 Apennines and Sicily (Italy). In: Geology of Italy (Eds U. Crescenti, S. D'Offizi, S. Merlino, L. Sacchi),  
231 Soc. Geol. Ital. Spec Vol, 32, Florence, 93–129
- 232 **Patacca, E. and Scandone, P.** (2007) Geology of the Southern Apennines. In: Results of the CROP Project,  
233 Sub-project CROP 04 Southern Apennines (Italy) (Eds Mazzotti, A., Patacca, E., and Scandone, P.),  
234 Boll. Soc. Geol. Ital. (Italian Journal of Geoscience), Spec. Publ., 7, 75–119.
- 235 **Patacci, M.** (2016) A high-precision Jacob's staff with improved spatial accuracy and laser sighting capability.  
236 Sedimentary Geology, **335**, 66-69.
- 237 **Peakall, J., McCaffrey, W.D. and Kneller, B.C.** (2000) A process model for the evolution, morphology, and  
238 architecture of sinuous submarine channels. Journal of Sedimentary Research, **70**(3), 434-448.
- 239 **Peakall, J. and Sumner, E.J.** (2015) Submarine channel flow processes and deposits: A process-product  
240 perspective. Geomorphology, **244**, 95-120.
- 241 **Pescatore, T.** (1978) Evoluzione tettonica del Bacino Irpino (Italia meridionale) durante il Miocene. Boll. Soc.  
242 Geol. Ital., **97**(5-6), 783-805.
- 243 **Pescatore, T.** (1988) La sedimentazione miocenica nell'Appennino campano-lucano. Soc. Geol. Ital. Mem.,  
244 **41**(1), 37-46.
- 245 **Pescatore, T., Salvati, G. and Tramutoli, M.** (1980) Regressive depositional cycles in the Gorgoglione flysch,  
246 Irpinids (Southern Italy). Geologica Romana, **19**, 51-61.
- 247 **Pescatore, T.S. and Senatore, M.** (1986) A comparison between a present-day (Taranto Gulf) and a Miocene  
248 (Irpinian Basin) foredeep of the Southern Apennines (Italy). In: Foreland Basins (Eds P.A. Allen and  
249 P. Homewood), Spec. Publ. Int. Assoc. Sediment., 8, 169–182.
- 250 **Pescatore, T., Renda, P., Schiattarella, M. and Tramutoli, M.** (1999) Stratigraphic and structural  
251 relationships between Meso-Cenozoic Lagonegro basin and coeval carbonate platforms in southern  
252 Apennines, Italy. Tectonophysics, **315**(1), 269-286.
- 253 **Pickering, K.T., Corregidor, J. and Clark, J.D.** (2015) Architecture and stacking patterns of lower-slope and  
254 proximal basin-floor channelised submarine fans, Middle Eocene Ainsa System, Spanish Pyrenees:  
255 An integrated outcrop–subsurface study. Earth-Science Reviews, **144**, 47-81.
- 256 **Piedilato, S. and Prosser, G.** (2005) Thrust sequences and evolution of the external sector of a fold and thrust  
257 belt: an example from the Southern Apennines (Italy). Journal of Geodynamics, **39**(4), 386-402.

- 258 **Pirmez, C., Beaubouef, R.T., Friedmann, S.J. and Mohrig, D.C.** (2000) Equilibrium profile and baselevel in  
259 submarine channels: examples from Late Pleistocene systems and implications for the architecture of  
260 deep-water reservoirs. In: Global deep-water reservoirs: Gulf Coast Section SEPM Foundation 20th  
261 Annual Bob F. Perkins Research Conference (pp. 782-805).
- 262 **Pitts, A., Casciano, C.I., Patacci, M., Longhitano, S.G., Di Celma, C. and McCaffrey, W.D.** (2017)  
263 Integrating traditional field methods with emerging digital techniques for enhanced outcrop analysis of  
264 deep-water channel-fill deposits. In: Sedimentology in Italy: recent advances and insights (Eds S.G.  
265 Longhitano, R.J. Steel, L. Pomar), Marine and Petroleum Geology, **87**, p.2-13.
- 266 **Porter, M.L., Sprague, A.R.G., Sullivan, M.D., Jennette, D.C., Beaubouef, R.T., Garfield, T.R., Rossen,**  
267 **C., Sickafoose, D.K., Jensen, G.N., Friedmann, S.J. and Mohrig, D.C.** (2006). Stratigraphic  
268 organization and predictability of mixed coarse- and fine-grained lithofacies successions in a lower  
269 Miocene deep-water slope-channel system, Angola Block 15. In: Giant hydrocarbon reservoirs of the  
270 world: From Rocks to reservoir characterization and modeling (Eds P.M. Harris and L.J. Weber),  
271 AAPG Memoir 88/SEPM Special Publication, p. 281–305.
- 272 **Posamentier, H.W. and Kolla, V.** (2003) Seismic geomorphology and stratigraphy of depositional elements  
273 in deep-water settings. *Journal of Sedimentary Research*, **73**(3), 367-388.
- 274 **Prather, B.E.** (2000). Calibration and visualization of depositional process models for above-grade slopes: a  
275 case study from the Gulf of Mexico. *Marine and Petroleum Geology*, **17**(5), 619-638.
- 276 **Prélat, A., Hodgson, D.M. and Flint, S.S.** (2009) Evolution, architecture and hierarchy of distributary deep-  
277 water deposits: a high-resolution outcrop investigation from the Permian Karoo Basin, South Africa.  
278 *Sedimentology*, **56**(7), 2132-2154.
- 279 **Pringle, J.K., Brunt, R.L., Hodgson, D.M. and Flint, S.S.** (2010) Capturing stratigraphic and sedimentological  
280 complexity from submarine channel complex outcrops to digital 3D models, Karoo Basin, South Africa.  
281 *Petroleum Geoscience*, **16**(4), 307-330.
- 282 **Pyles, D.R., Jennette, D.C., Tomasso, M., Beaubouef, R.T. and Rossen, C.** (2010) Concepts learned from  
283 a 3D outcrop of a sinuous slope channel complex; Beacon Channel Complex, Brushy Canyon  
284 Formation, West Texas, U.S.A. *Journal of Sedimentary Research*, **80**(1-2), 67-96.
- 285 **Romans, B.W., Fildani, A., Hubbard, S.M., Covault, J.A., Fosdick, J.C. and Graham, S.A.** (2011) Evolution  
286 of deep-water stratigraphic architecture, Magallanes Basin, Chile. *Marine and Petroleum Geology*,  
287 **28**(3), 612-628.
- 288 **Roure, F.** (2008) Foreland and Hinterland basins: what controls their evolution? In: *Orogenic Processes in the*  
289 *Alpine Collision Zone* (pp. S5-S29). Birkhäuser, Basel.
- 290 **Samuel, A., Kneller, B., Raslan, S., Sharp, A. and Parsons, C.** (2003) Prolific deep-marine slope channels  
291 of the Nile Delta, Egypt. *AAPG Bulletin*, **87**(4), 541-560.
- 292 **Schwarz, E. and Arnott, R.W.C.** (2007) Anatomy and evolution of a slope channel-complex set  
293 (Neoproterozoic Isaac Formation, Windermere Supergroup, southern Canadian Cordillera):  
294 implications for reservoir characterization. *Journal of Sedimentary Research*, **77**(2), 89-109.

- 295 **Stevenson, C.J., Talling, P.J., Wynn, R.B., Masson, D.G., Hunt, J.E., Frenz, M., Akhmetzhanov, A. and**  
296 **Cronin, B.T.** (2013) The flows that left no trace: Very large-volume turbidity currents that bypassed  
297 sediment through submarine channels without eroding the sea floor. *Marine and Petroleum Geology*,  
298 **41**, 186-205.
- 299 **Stevenson, C.J., Jackson, C.A.L., Hodgson, D.M., Hubbard, S.M. and Eggenhuisen, J.T.** (2015) Deep-  
300 water sediment bypass. *Journal of Sedimentary Research*, **85**(9), 1058-1081.
- 301 **Stright, L., Stewart, J., Campion, K. and Graham, S.** (2014) Geologic and seismic modeling of a coarse-  
302 grained deep-water channel reservoir analog (Blacks Beach, La Jolla, California). *AAPG Bulletin*,  
303 **98**(4), 695-728.
- 304 **Sylvester, Z., Pirmez, C. and Cantelli, A.** (2011) A model of submarine channel-levee evolution based on  
305 channel trajectories: Implications for stratigraphic architecture. *Marine and Petroleum Geology*, **28**(3),  
306 716-727.
- 307 **Sylvester, Z. and Covault, J.A.** (2016) Development of cutoff-related knickpoints during early evolution of  
308 submarine channels. *Geology*, **44**(10), 835-838.
- 309 **Talling, P.J., Masson, D.G., Sumner, E.J. and Malgesini, G.** (2012) Subaqueous sediment density flows:  
310 depositional processes and deposit types. *Sedimentology*, **59**(7), 1937-2003.
- 311 **Thomas, M.F.H. and Bodin, S.** (2013) Architecture and evolution of the Finale channel system, the Numidian  
312 Flysch Formation of Sicily; insights from a hierarchical approach. *Marine and Petroleum Geology*, **41**,  
313 163-185.
- 314 **Van der Merwe, W.C., Hodgson, D.M., Brunt, R.L. and Flint, S.S.** (2014) Depositional architecture of sand-  
315 attached and sand-detached channel-lobe transition zones on an exhumed stepped slope mapped  
316 over a 2500 km<sup>2</sup> area. *Geosphere*, **10**(6), 1076-1093.
- 317 **Vezzani, L., Festa, A. and Ghisetti, F.C.** (2010) Geology and Tectonic Evolution of the Central-Southern  
318 Apennines, Italy. *Geological Society of America Special Papers*, 469, 1- 58.
- 319 **Wynn, R.B., Kenyon, N.H., Masson, D.G., Stow, D.A. and Weaver, P.P.** (2002) Characterization and  
320 recognition of deep-water channel-lobe transition zones. *AAPG Bulletin*, **86**(8).

321 FIGURES

322

323

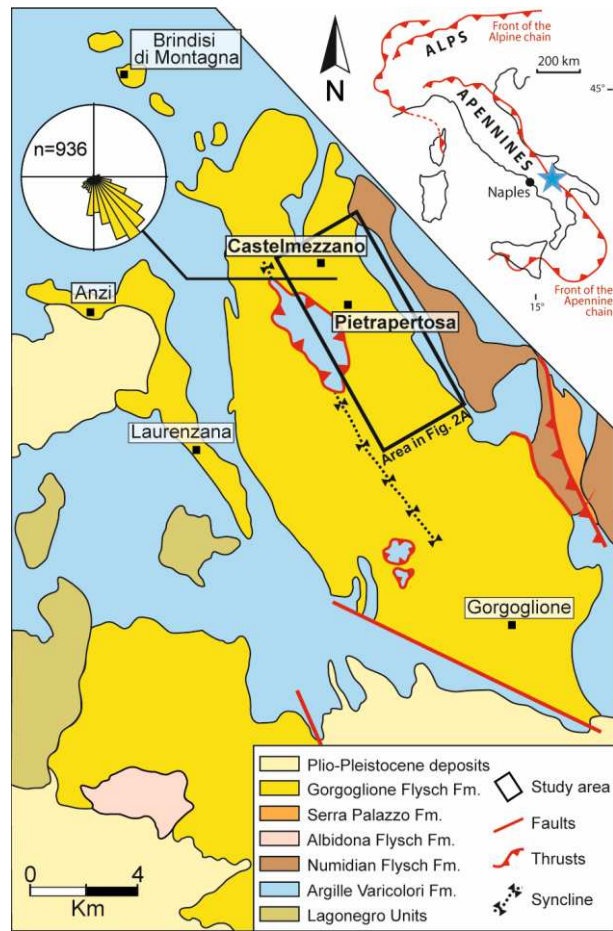
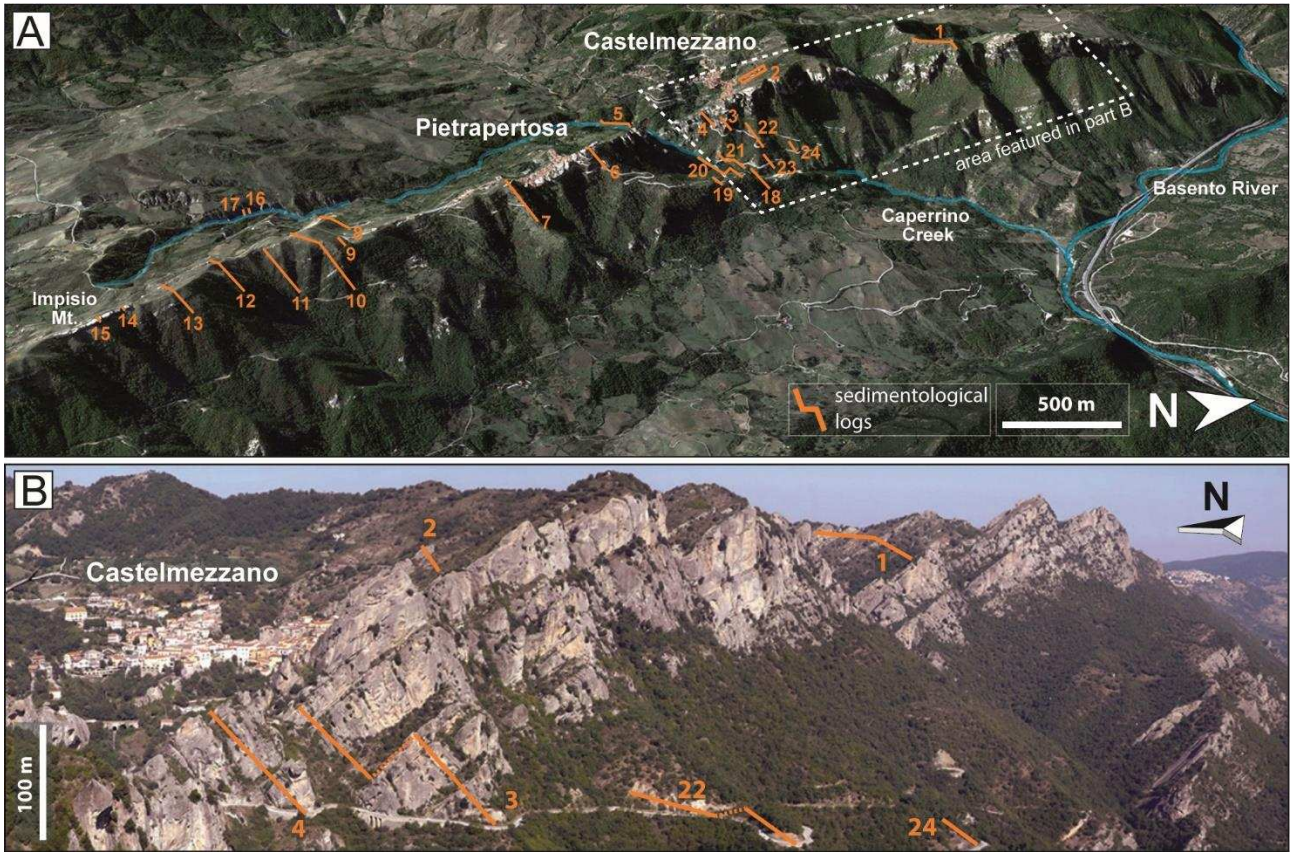


Figure 1



324

325

Figure 2

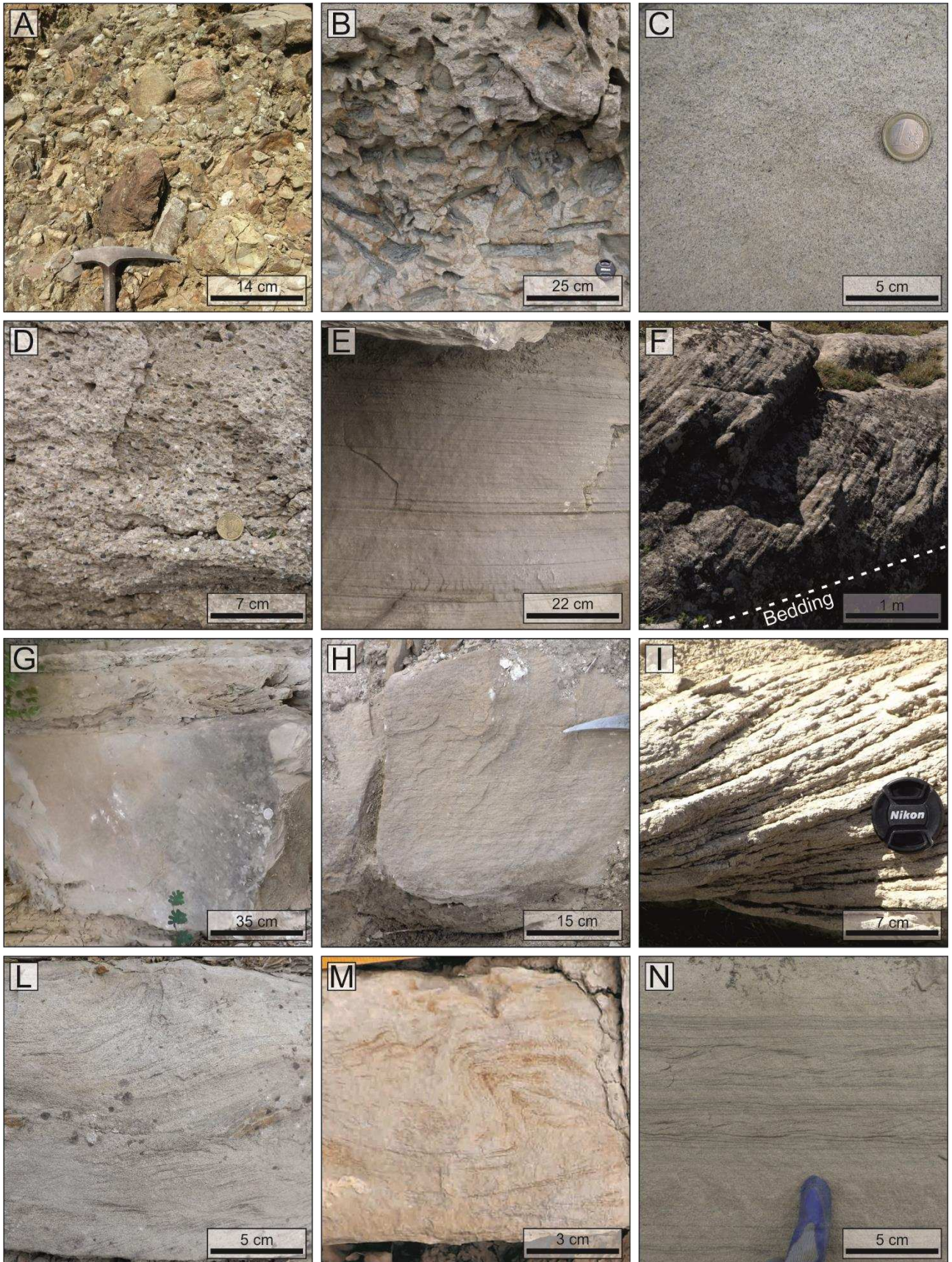


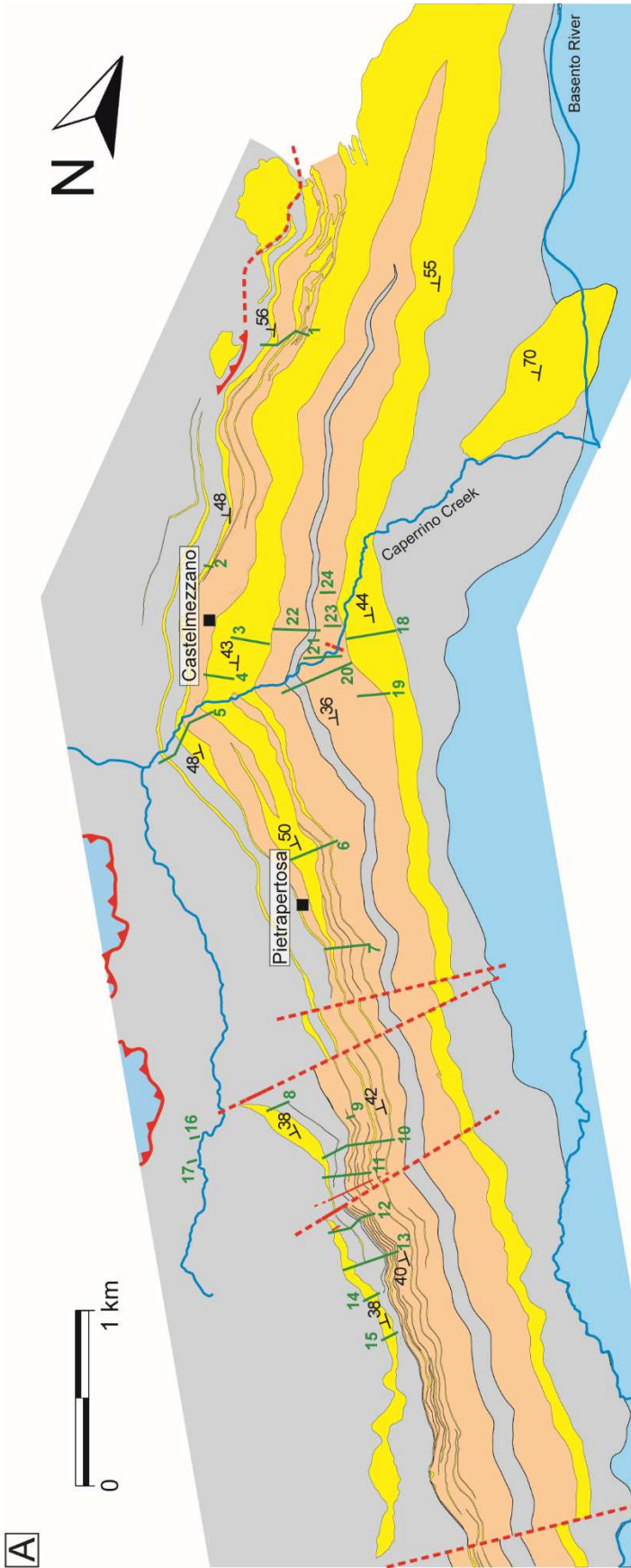
Figure 3

326

327

328

329



GORGOLGIONE FLYSCH Fm. (Miocene)

- F.A.1 - coarse-grained sandstones and conglomerates
- F.A.2 - sand-prone heterolithic deposits
- F.A.3 - mud-prone heterolithic deposits

ARGILLE VARICOLORI Fm. (Cretaceous - Eocene)

- faults
- thrusts
- bedding
- log

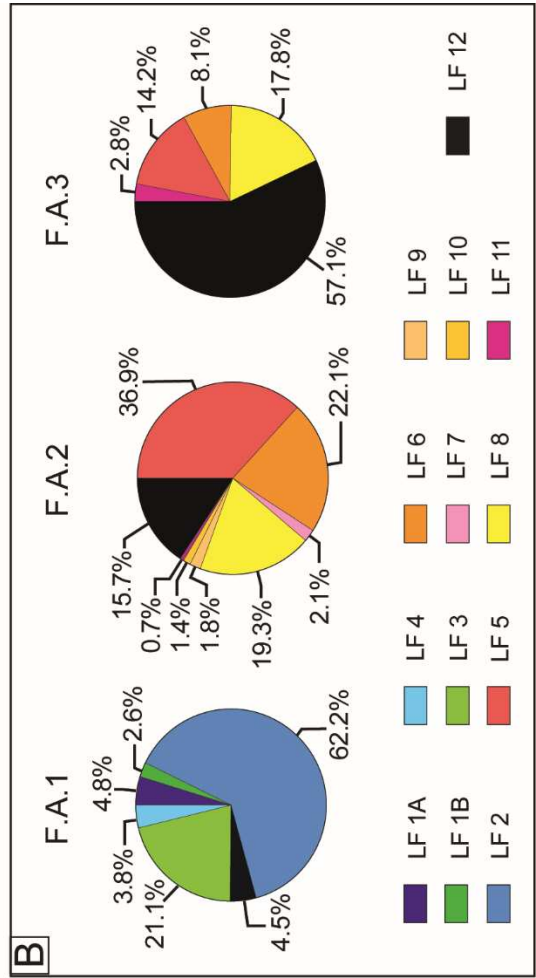
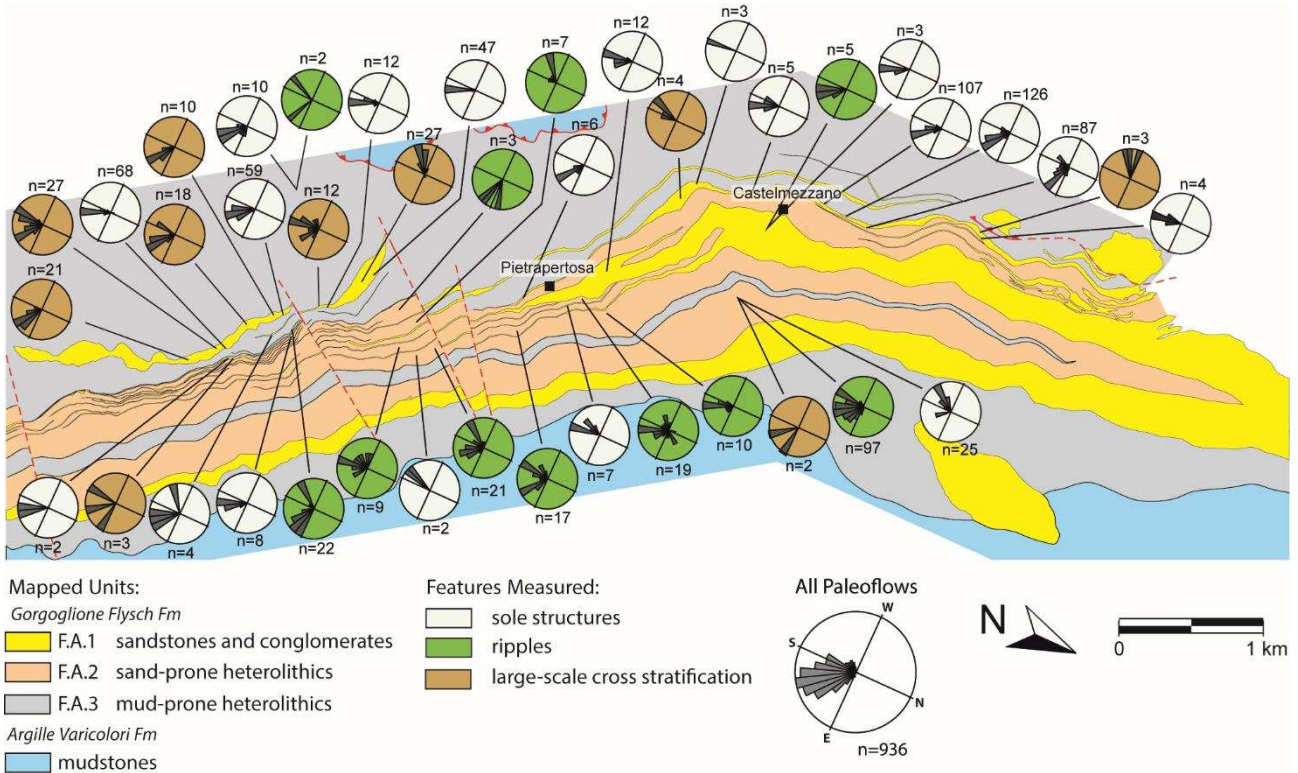


Figure 4

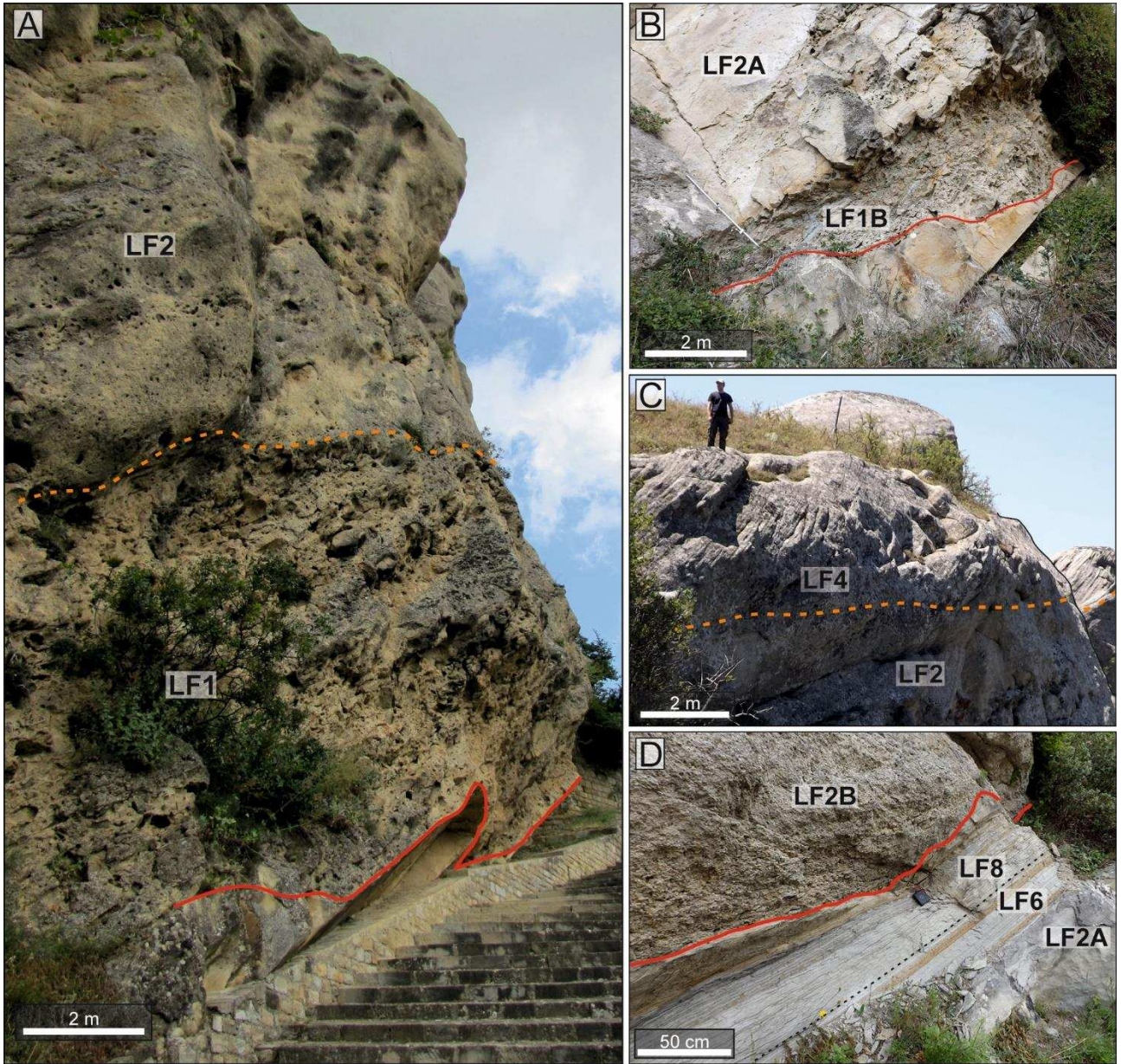


330

331

332

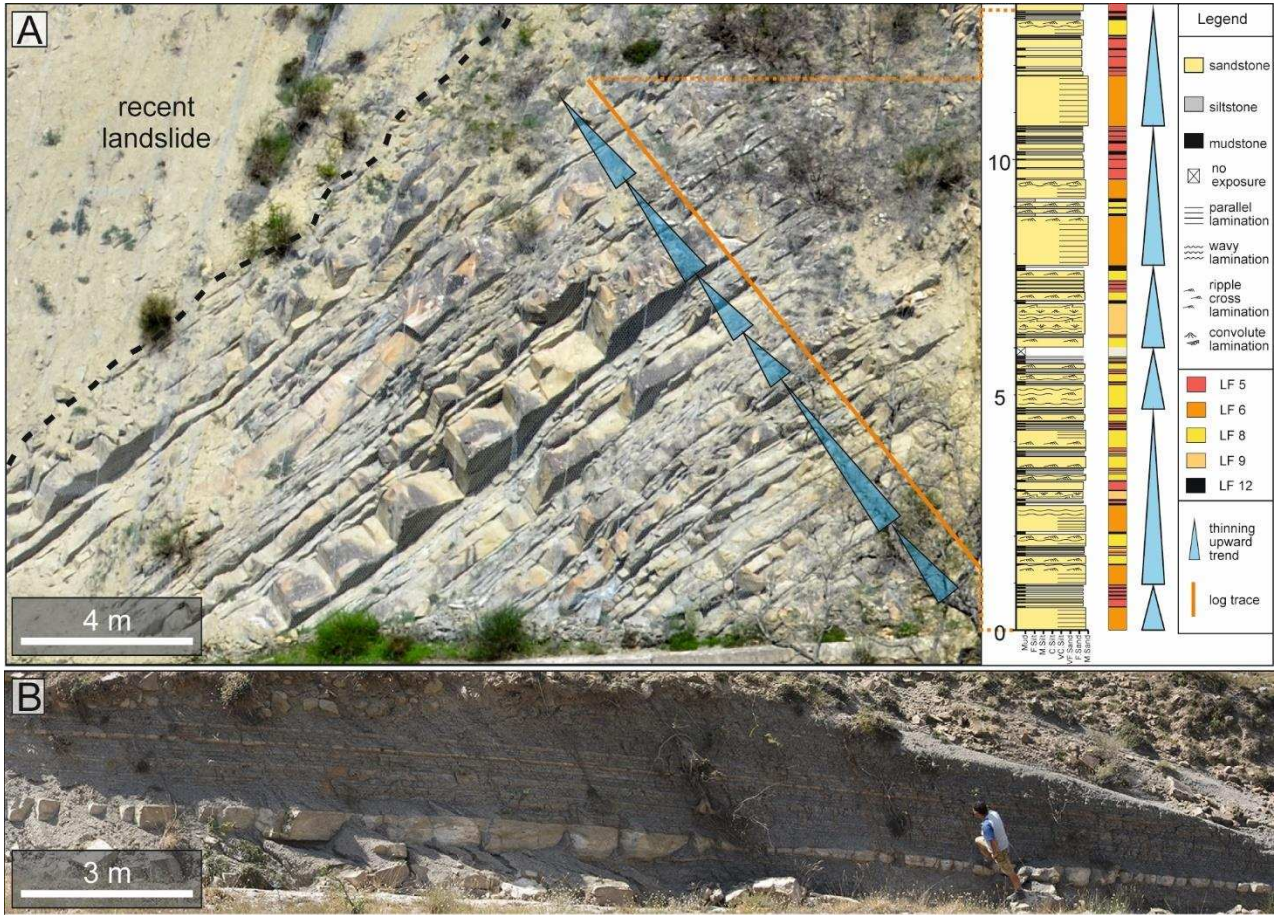
Figure 5



333

334

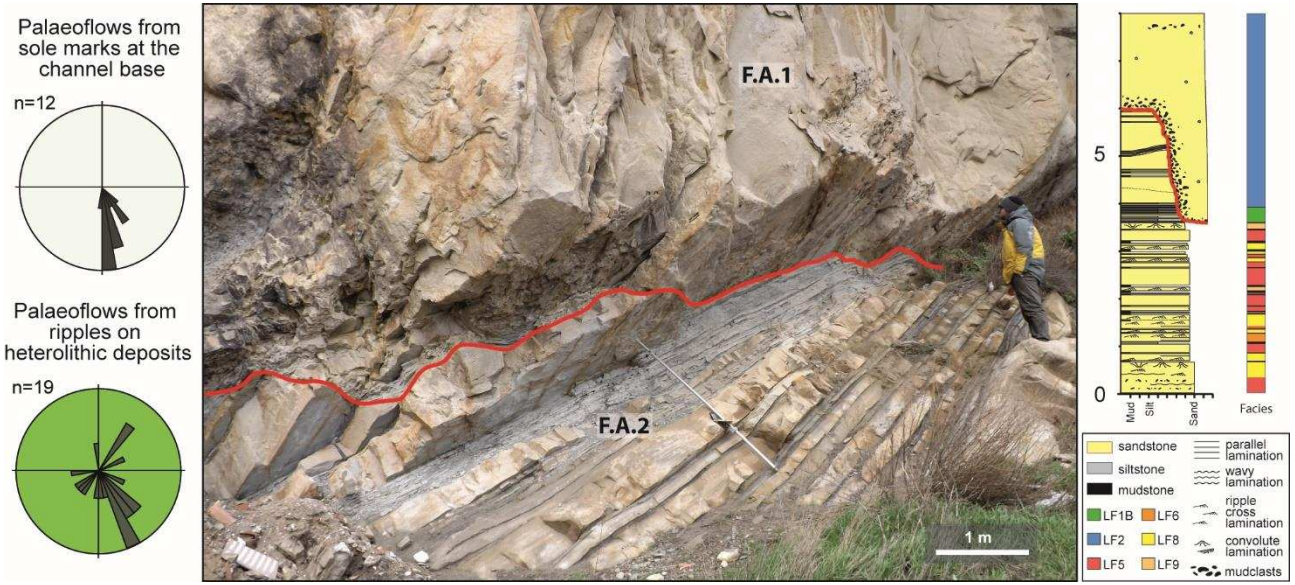
Figure 6



335

336

Figure 7



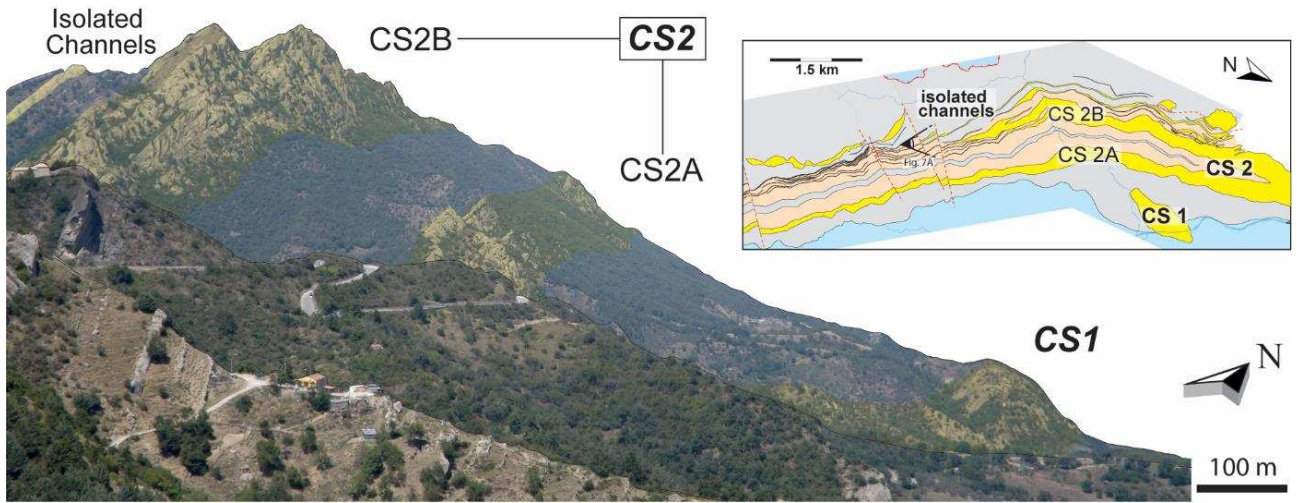
337

338

339

Figure 8

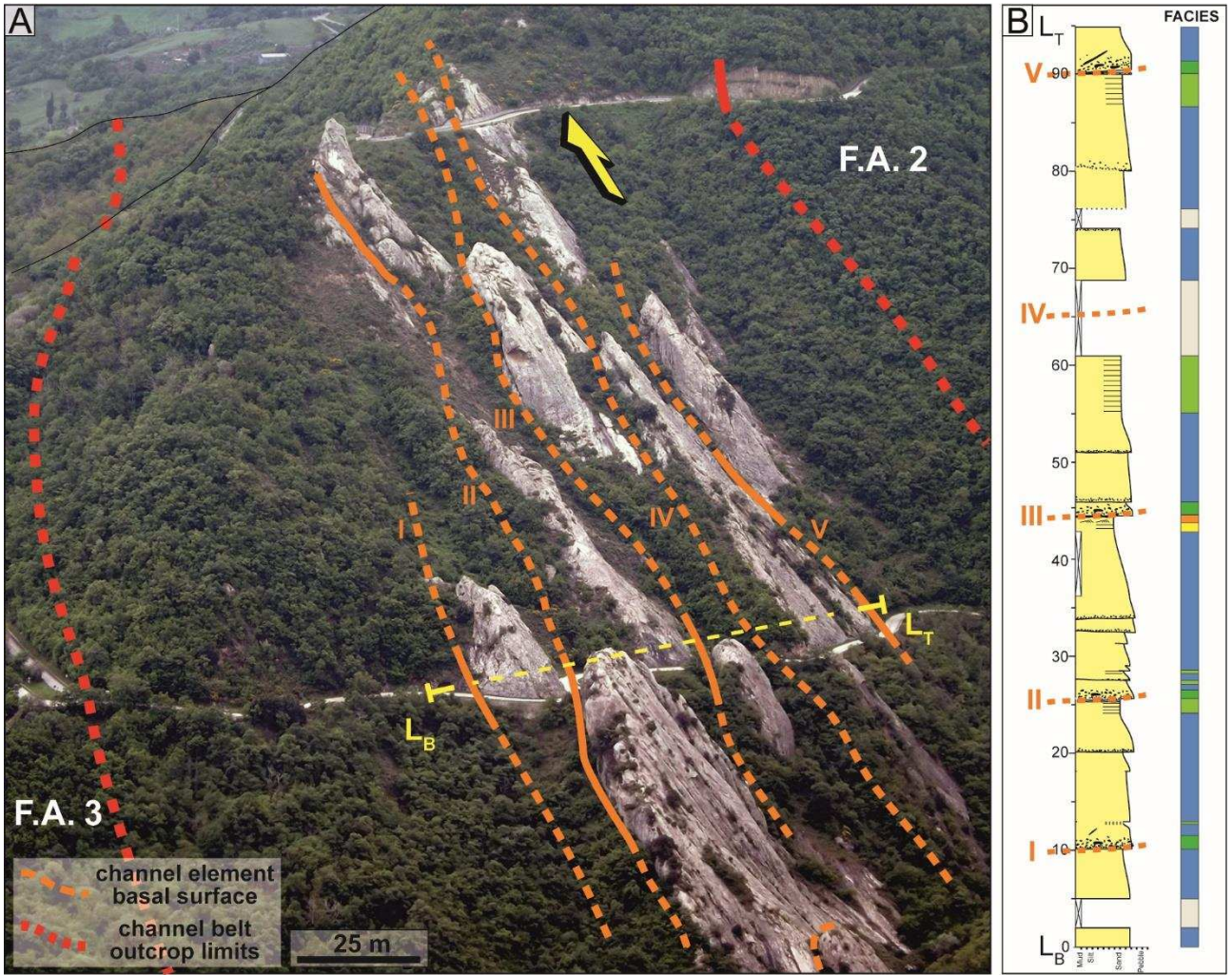




343

344

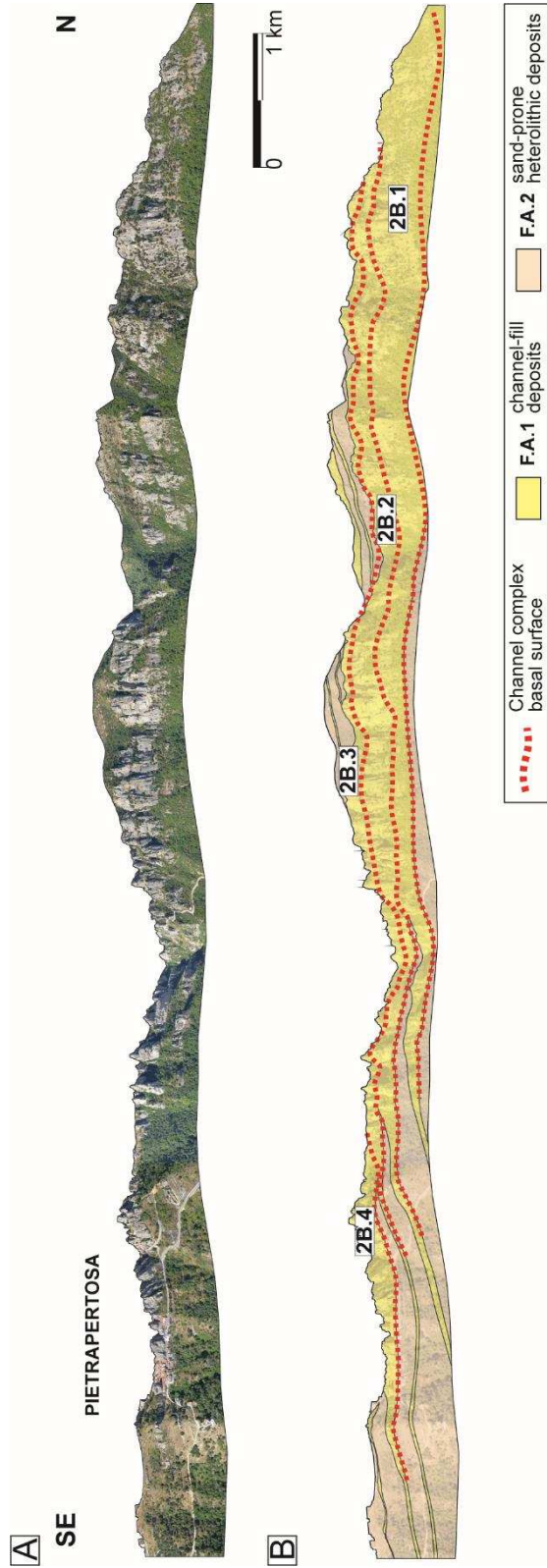
Figure 10



345

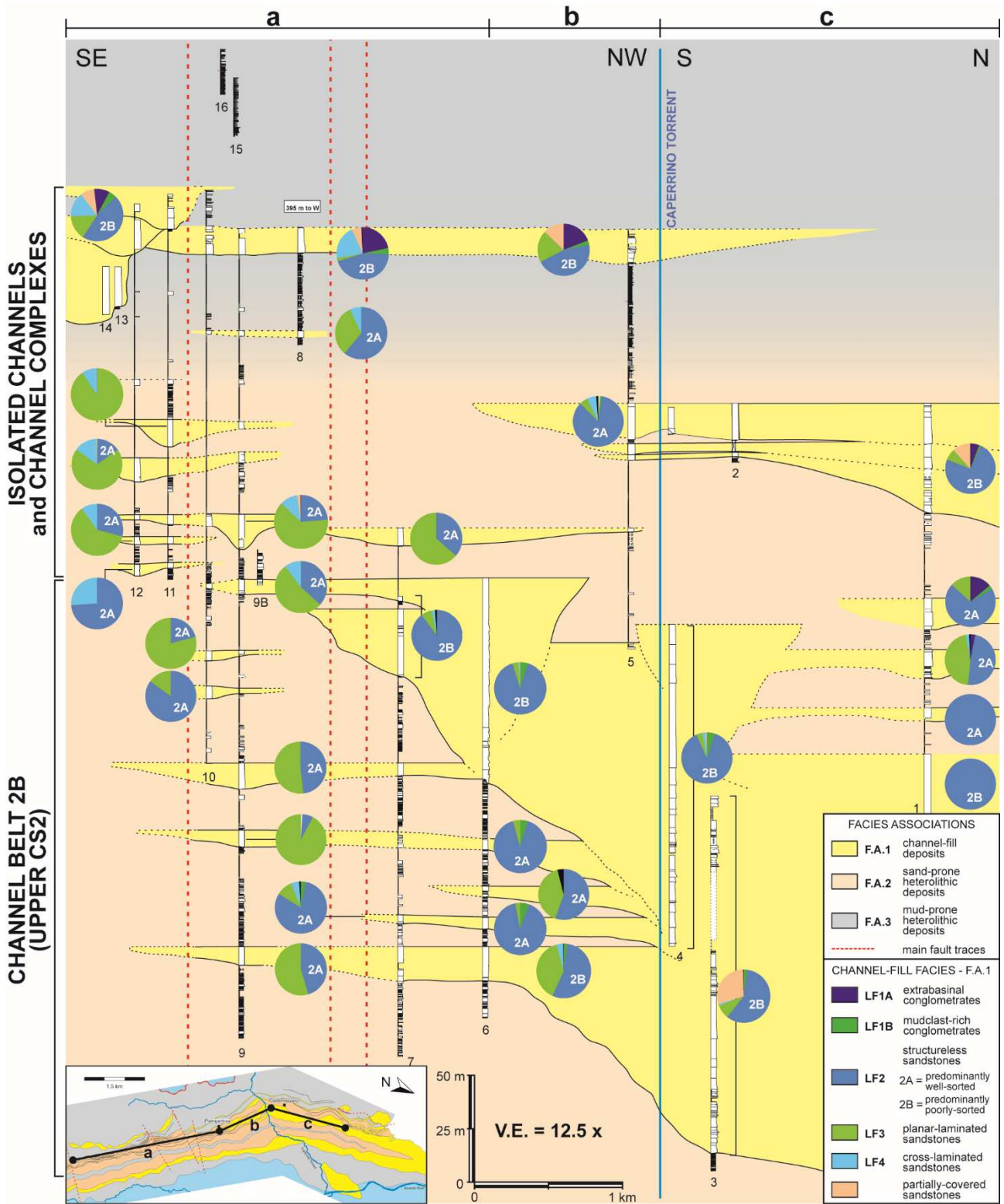
346

Figure 11



347

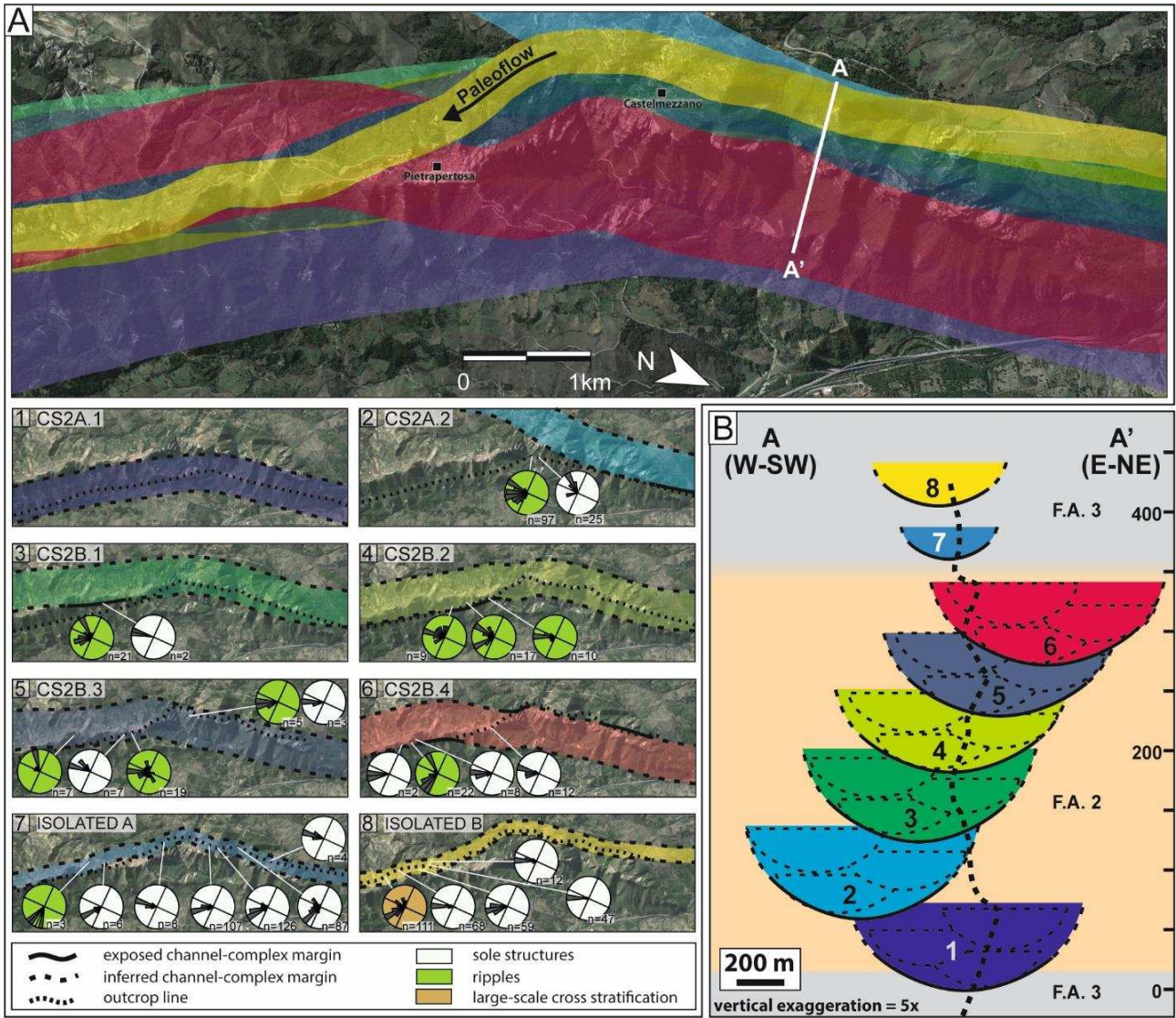
348 Figure 12



349

350

Figure 13



351

352

Figure 14

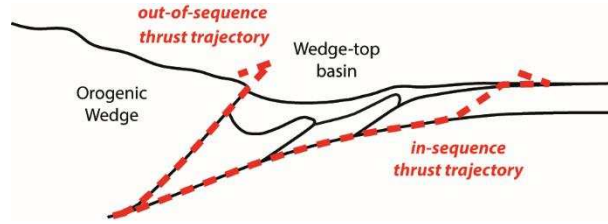


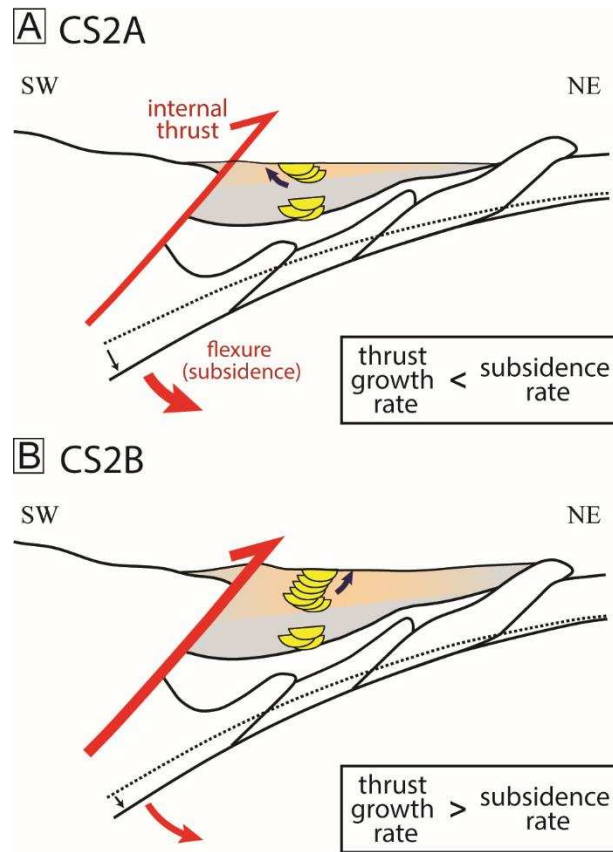
Figure 15

353

354

355

356



357

358

Figure 16

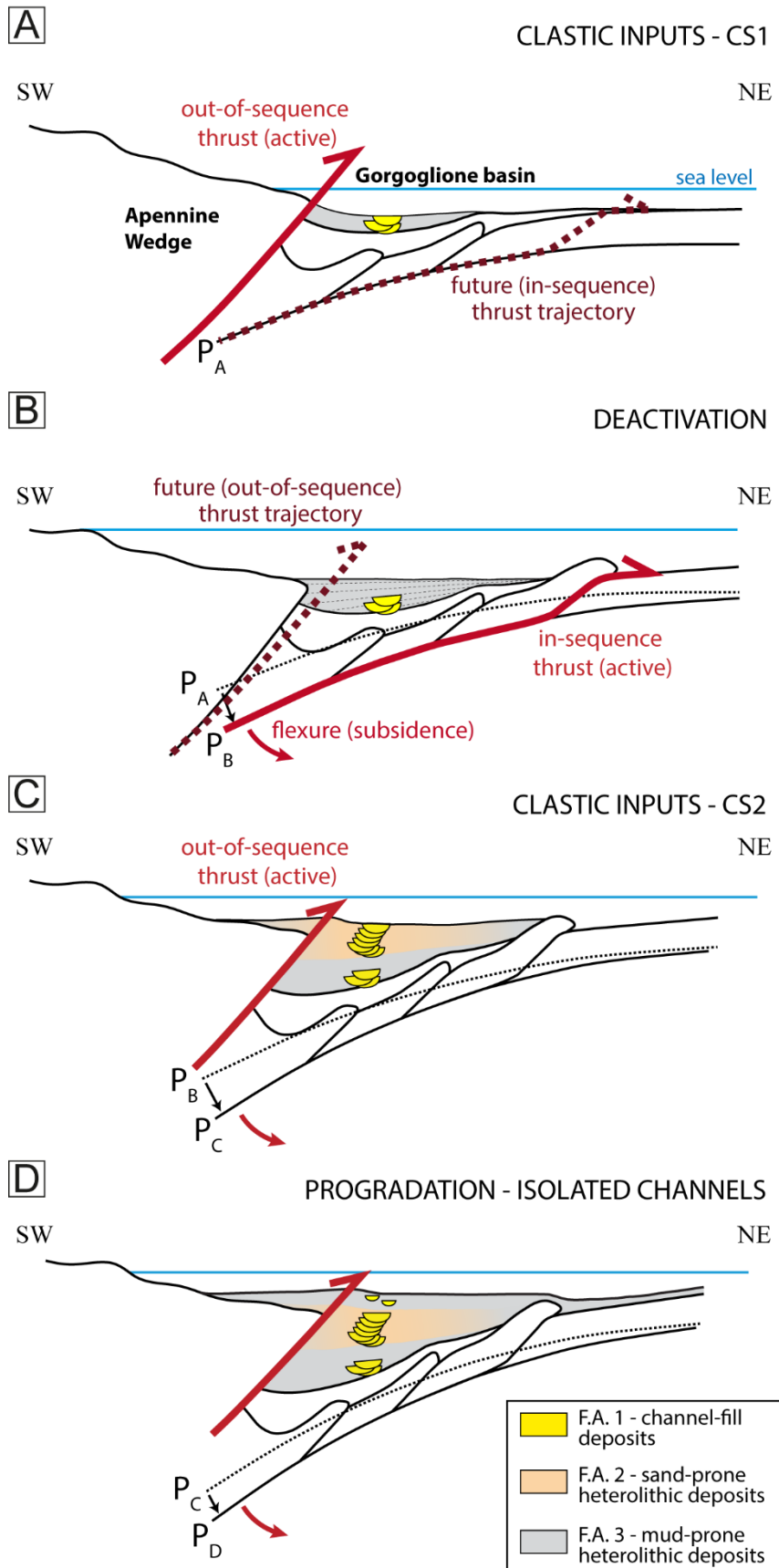


Figure 17

359

360

## CAPTIONS

Figure 1 - Schematic geological map of the main outcrops of the Gorgoglione Flysch (GF) Formation (from Critelli and Loiacono 1988, modified). Proximal facies are recognized in the western outcrops, at Brindisi di Montagna, Anzi and Laurenzana, where the GF is characterized by very coarse-grained sandstones and conglomerates derived from internal paleogeographic domains. The main depocentral area is located to the east, between the towns of Castelmezzano and Gorgoglione, where the GF succession reaches a thickness of nearly 2000 m. The regional paleoflow is towards southeast.

Figure 2 – A) Overview of the study area (see Fig. 1 for location), extending for about 15 km between the Basento River to the north and the Impisio Mountain to the south. Multiple stratigraphic sections have been measured across the outcrop belt, in order to characterize spatial changes in architectural and sedimentological features. B) The monoclinical configuration of the GF formation, dipping towards SW of nearly 40°, which defines the spectacular cliffs that inspired the local name of “Lucanian Dolomites” (location in A).

Figure 3 – Lithofacies of the GF formation. (A) LF1A, matrix-supported extrabasinal conglomerates. (B) LF1B, mudclasts conglomerate. (C) LF2A, clean, poorly-sorted coarse-grained sandstones. (D) LF2B, very coarse-grained sandstones with dispersed granule- to pebble-sized clasts. (E) LF3, planar-laminated sandstones. (F) LF4, coarse-grained sandstones with large-scale cross-stratification. (G) LF5, massive, medium-grained sandstones (Bouma Ta). (H) LF6, planar-laminated, medium-bedded sandstones (Bouma Tb). (I) LF7, cross-stratified, medium bedded sandstones. (L) LF8, ripple cross-laminated, thin-bedded sandstones (Bouma Tc). (M) LF9, convoluted, fine-grained sandstones. (N) LF10, alternating planar-laminated (Tb) and ripple cross-laminated (Tc) fine-grained sandstones.

Figure 4 – A) Geological map of the study area (see Fig. 1 for location), showing the distribution of the three main facies associations. The turbidite succession is affected by post-depositional deformation characterized by large-scale tilting and by smaller structures of various ages (e.g., normal faults in the southern portion of the study area). The GF Formation unconformably overlies the Argille Varicolori Formation (Cretaceous-Eocene). In addition, the Argille Varicolori Formation overthrusts the GF Fm, bounding the turbidite succession at the top. B) Pie charts of the relative proportions of sedimentary facies (codes as in Table 1) across the study area, calculated as thickness percentages from all the logged sections. Net-to-gross values (N:G) represent the cumulative thickness of sandstones versus the total thickness.

Figure 5 – Paleoflow rose diagrams distinguished by location and typology of measured features, overlain on the geological map of fig. 4A. Note that the vector mean for all the 936 measurements is N 152° (southeast).

Figure 6 – Channel-fill deposits (F.A.1). (A) Matrix-supported, mixed extrabasinal and intra-basinal conglomerates (LF1) overlaid by poorly-sorted structureless sandstones (LF2B), characteristic of channel axis (B) Basal lag conglomerates almost entirely constituted of mudclasts (LF1B) and overlain by clean massive sandstones (LF2A), characteristic of channel off-axis. (C; D) Variable character of the top of channel-fill sequences. In (C), thick structureless sandstones (LF2) are abruptly overlain by large-scale cross-stratified sandstones (LF4). Conversely, in (D) amalgamated, fine-grained structured sandstones (LF6 and LF8) are truncated by an extensive erosional surface marking the beginning of the subsequent channel-fill sequence.

Figure 7 – Heterolithic, out-of-channel deposits. A) Thinning-upward trends (blue triangles) within the sand-prone heterolithic deposits of F.A.2. The section is partially covered by collapsed material. B) Lenticular bed composed of massive sandstones (LF5) embedded in mud-prone heterolithic deposits of F.A.3.

Figure 8 – Heterolithic, sand-prone, thin bedded deposits of F.A.2, incised by concave-up surfaces that confine F.A.1 packages. F.A.2 deposits in the study area are typically documented adjacent to F.A.1 channel fill strata, but outside their basal erosion surfaces. Paleoflow indicators in F.A.2 packages record variable flows, diverging from the measurements from the adjacent channels. These features suggest that F.A.2 deposits can be interpreted as overbank deposits.

Figure 9 – Elementary channel architectures documented in the GF succession with field examples (locations in the inset geological map). A) Weakly confined channels commonly display widths > 450m and range in thickness from 9 to 17 m and are typically flanked by sand-prone heterolithic deposits of F.A.2. The reported example is from a weakly-confined channel exposed below the town of Pietrapertosa. Its base (in red) has been walked and mapped in detail. The typical elongate geometries of the turbidite channels in the GF succession are an apparent effect of the oblique outcrop belt orientation relative to the paleoflow. B) Incisional channels cut deeply into mud-prone heterolithic deposits of F.A.3. These sandbodies are typically 180 to 450 m wide and up to 26 m thick, as shown by the example, the “cemetery channel”, an isolated channel element in the upper part of the succession.

Figure 10 – A) Panoramic view of the GF succession in the study area, showing the main large-scale architectural units: channel complex-sets and isolated channels (see inset map for location). In this study, channel belts 2A and 2B are considered as parts of the same migrating channel complex-set, referred to as “CS2”.

Figure 11 – A) Stacked elementary channels of CS2A, 16 to 19 m thick, exposed along the valley of the Caperrino Creek. CS2A overlies a prominent erosional surface, deeply incisional into mud-prone heterolithic deposits (F.A.3). The regional paleoflow is towards SSE (yellow arrow). B) Sedimentological log  $L_B - L_T$  of CS2A (see Fig. 7A for the log legend and Fig. 4B for the facies legend). Erosional surfaces at the base of the individual channel elements are mantled by thick intervals of matrix-supported mudclast-rich conglomerates (LF1B). This section exposes the stacked channel axes, which are dominated by pebble-rich structureless sandstones (LF2B), with subordinate clean massive sandstones (LF2A) and planar laminated sandstones (LF3), locally capped by large-scale cross stratified sandstones (LF4) and structured fine-grained sandstones (LF6 and LF8).

Figure 12 – Aerial photopanel (A) and interpretation (B) of the northern sector of CS2B. Four amalgamated channel-complexes, 60 to 85 m thick, have been recognized, separated by major erosional surfaces laterally traceable for about 4 km across the study area. Channel complexes show an abrupt lateral thinning toward S-SE. The apparent elongated shape of the channel belt is due to the highly oblique orientation of the outcrops, which is nearly parallel to the regional paleoflow direction (toward SSE).

Figure 13 – Correlation panel of the upper portion of the GF succession exposed in the study area, showing the spatial distribution of the four channel-fill facies (F.A.1). Location in the inset geological map; offset of post-depositional faults (dashed red lines) has been removed. The panel includes CS2B and the upper isolated channels and channel complexes. Channel-fill deposits in the northern sector of CS2B are dominated by amalgamated LF2B sandstones and exhibit a lateral transition towards SE into less-amalgamated and laterally-persistent sandbodies with abundant LF2A and LF3 sandstones alternating with very thin beds of mudstones (LF12). Due to the oblique orientation of the outcrop belt relative to the paleoflow, depositional geometries of the sandbodies appear considerably stretched and elongated. That said, the facies distribution suggests that CS2B is comprised of stacked and amalgamated, weakly-confined channels. The lateral facies trend has been interpreted to reflect a progressive transition from channel axis to channel margin facies. The correlation panel highlights the upward change in the character of the heterolithic deposits, which passes from sand-prone (F.A.2) to mud-prone (F.A.3). Vertical exaggeration 12.5 times.

Figure 14 – A) Schematic reconstruction of the planform geometry of the channel complexes comprising the CS2 and of two isolated channel elements in the upper part of the GF succession. The topographic map in the background represents the distribution of the channel-fill deposits in the study area. Due to the lack of exposure of the channel complex-set at both margins of CS2, the real width of its component channel complexes cannot be measured directly. A constant channel complex width of ~1 km has been considered from the combination of minimum widths from field observations and widths of comparable deep-water channel complexes in the literature (e.g., Campion et al., 2005; Stright et al., 2014). The regional paleoflow was roughly SE-ward, with limited variability; hence, individual channelized units are interpreted as having a relatively low degree of sinuosity. CS1 is not represented due to the lack of paleoflow measurements and discontinuous

exposures of channel fill deposits. B) Cross section orthogonal to regional paleoflow direction (location in A), chosen to show the stacking pattern of the different units in the northern portion of the turbidite system. The dotted black line shows the outcrop profile in the transect line. On the assumption that the inferred scale of lateral channel movement is correct, it can be inferred that CS2 is dominated by vertical aggradation, with limited lateral migration of the component units. The symmetric cross-sectional channel-fill architecture is a simplification based on the inferred low sinuosity of the channelized units.

Figure 15 – Schematic representation of the two main trajectories followed by the active thrusts in the Apennine thrust-and-fold belt (Patacca and Scandone, 2007). The inner trajectory (i.e., out-of-sequence thrust) crosses the base of the growing orogen. The outer trajectory (i.e., in-sequence thrust) which moves the front of the accretionary wedge. Thrusts activate alternatively along these trajectories, defining the inner and the outer margins of the wedge-top basin, respectively.

Figure 16 - Schematic representation of the progressive, limited lateral migration of CS2 depocenter in GF basin. This characteristic migration pattern might be interpreted as the net result of the competition between the growth of the internal thrust and the regional subsidence, which created accommodation space at a constant rate and promoted aggradation. A) When the growth rate of the thrust was lower than the subsidence rate, the fast eastward roll-back at the hinge of the subduction zone favored the migration of the channel system depocentre towards SW; B) Conversely, when the thrust growth rate became higher than the subsidence rate, the tilt associated with the push of this regional tectonic structure forced the CS2 to shift towards NE.

Figure 17 – Main stages of the GF turbidite system evolution, developed during the Late Miocene in a thrust-top basin of the Southern Apennines. Significant accommodation space was formed as a consequence of the increasing subsidence of the basin, associated to the progressive flexure of the subducting plate. A) The early activity of the internal thrusts determined increasing gradients in the orogenic hinterland, promoting the establishment of a slope environment. High slope gradients facilitated the initiation and development of the incisional gravity flows that built up CS1. B) The subsequent activation of the outer thrusts progressively configured a narrow basin, marking the end of CS1 sedimentation and promoting the deposition of a thick package of F.A.3 deposits. Decreasing slope gradients in the orogenic hinterland led to a gradual restoration of a base-of-slope environment. C) The re-activation of the internal thrusts restored the coarse clastic inputs in the basin and fostered the development of CS2. D) Ongoing coarse-grained inputs, combined with a gradual increase of the basinal slope gradient, promoted the formation of progressively more incisional turbidity currents. Accordingly, the amalgamated, weakly confined channels of the CS2 gradually evolved into isolated, incisional channels. This upward change in channel architectural style is interpreted to represent the progradation of a slope channel system over a weakly-confined, sand-prone channel system on the near base-of-slope.

Table 1 – Operative lithofacies recognized in the Gorgoglione Flynch Formation. Turbidite divisions are from Bouma (1962), Lowe (1982) and Mutti (1992).

Table 2 – Main features of the elementary channel architectures recognized in the GF succession.

FACIES	LITHOLOGY	GRADING	THICKNESS	PHYSICAL STRUCTURES	LITHOLOGICAL ACCESSORIES	BASAL SURFACE PROPERTIES	TURBIDITE DIVISION	PROCESS INTERPRETATION
<b>LF1</b> Matrix-supported conglomerates	LF1A: pebble to boulder extrabasinal conglomerate with coarse to very coarse sandstone matrix  LF1B: pebble to cobble mudclast conglomerate with very coarse sandstone matrix	Typically ungraded and disorganized. Local weak normal grading	LF1A usually 2.1 - 2.9 m range 0.4 - 5.2 m  LF1B usually 0.5 - 2.3 m range 0.2 - 3.4 m	Chaotic internal organisation. Sole structures (flute and groove casts)	LF1A: sub-rounded to sub-angular extraformational clasts, 6 - 80 cm in diameter (average 20 cm).  LF1B: angular to sub-rounded (mainly disk-shaped) mudclasts, 1 - 30 cm in diameter. Local substrate blocks up to 1.5 m	Sharp and irregularly-shaped, often concave upward, erosional	-	Lag deposits from bypassing high-density turbidity currents. Bed-load transport from highly-incisional flows. LF1B mudclasts incorporated into the bypassing flow after turbulent scouring of cohesive mud substrate
<b>LF2</b> Structureless, thick bedded sandstones	LF 2A: medium to very coarse, well-sorted sandstone  LF2B: medium to very coarse, poorly-sorted sandstone	Ungraded to crudely normally graded	usually 0.9 - 2 m range 0.6 - 5.5 m  Amalgamated beds locally form units up to 53 m thick	Structureless, with local dewatering features	LF2A: disk-shaped mudclasts, 1 to 6 cm in diameter  LF2B: extrabasinal clasts, up to 5 cm in diameter, locally in lags	Sharp to undulating. Commonly amalgamated, marked by aligned mudclasts. Locally gradational with underlying facies	S3 ; F5	Rapid deposition of suspended sediment from collapsing, high-density currents with high sediment fallout rates, suppressing bed-load traction

<b>LF3</b> Planar-laminated, thick bedded sandstones	Medium to coarse, clean sandstone	Ungraded to normally-graded	usually 0.6 - 1.7 m range 0.4 - 3.25 m  Amalgamated beds locally form units up to 11.2 m thick	Closely- spaced planar laminations	Aligned mudclasts, up to 5 cm in diameter	Planar. Commonly gradational with underlying facies.  Locally amalgamated, marked by aligned mudclasts	T <sub>t</sub> ; F7	Deposition from high-concentration near-bed layers (traction carpets) generated by rapid sediment-fallout and progressive traction beneath high-density flows
<b>LF4</b> Large-scale, cross-stratified sandstones	Medium to coarse, clean sandstone	Normally graded	usually 0.6 - 1.4 m range 0.3 - 6.4 m	Multiple sets of large-scale 3D cross stratifications	Local seams of broadly aligned cm-sized rip-up mudstone clasts separating different bedsets	Commonly sharp, locally gradational	F6	Gradual decrease of confinement of sandy dense flows, leading to fast and lower-concentration, fully turbulent tractive flow
<b>LF5</b> Massive, thin-bedded sandstones	Fine to medium sandstone	Typically ungraded or slightly normally graded	1 - 45 cm (occasionally up to 1.3 m)	Structureless, with occasional planar laminations or ripples at the top	Occasional cm-sized aligned mudclasts. Rare extrabasinal clasts up to 1 cm	Typically planar; sporadically weakly erosional, ornamented by small flutes	T <sub>a</sub> , with local T <sub>ab</sub> , T <sub>abc</sub>	Rapid deposition from high density turbidity currents with very high sediment-fallout rates, preventing the formation of tractive features
<b>LF6</b> Planar laminated, thin-bedded sandstones	Fine to medium, clean sandstone	Ungraded to normally graded	6 - 75 cm (occasionally up to 90 cm)	Closely- spaced planar laminations, with local ripples or wavy laminations at the top	None	Planar	T <sub>b</sub> , with local T <sub>bc</sub>	a) deposition from low amplitude bed waves in waning and dilute, low-density flows, under

								low suspension fallout rates;  b) deposition from traction carpets beneath high-density flows
<b>LF7</b> Cross laminated, thin-bedded sandstones	Fine to medium, clean sandstone	Ungraded to normally graded	12 - 64 cm (occasionally up to 87cm)	Small- to medium-scale, low-angle cross stratification, with stratasesets ranging from 22 to 60 cm thick	None	Planar, with undulated tops	-	Deposition from dilute flows, with very low sediment fallout rates
<b>LF8</b> Ripple cross laminated, thin-bedded sandstones	Predominantly fine, clean sandstone, sometimes up to medium sandstone	Normally graded from fine sandstone at the base to siltstone	1 - 45 cm (occasionally up to 80 cm)	Ripples or wavy laminations	None	Planar, with undulated tops	T <sub>c</sub> , with local T <sub>cd</sub>	Deposition from waning, relatively diluted and fully turbulent suspensions, with low rates of sediment fallout
<b>LF9</b> Convolute, thin-bedded sandstones	Predominantly fine, clean sandstone, sometimes up to medium sandstone	Normally graded from fine sandstone at the base to siltstone	3 - 17 cm (occasionally up to 60 cm)	Convolute laminations	None	Planar, with undulated tops	T <sub>c</sub>	Very rapid deposition of fine-grained sediment, triggering syn- and post-depositional upward dewatering
<b>LF10</b> Vacillatory turbidites	Fine to medium, clean sandstone	Ungraded	9 - 48 cm (occasionally up to 83 cm). Rare amalgamation to	Alternating planar laminations and ripples or wavy laminations	None	Planar, with undulated tops	T <sub>bcbc</sub>	Flow regime fluctuations of a tractive, low-density turbidity current

			form units up to 2.3 m thick					
<b>LF11</b> Deformed deposits	Fine- to medium sandstone blocks or beds in a mudstone or sandstone matrix	Ungraded	32 - 250 cm	Folded and contorted beds with minor thrusts and dewatering	Locally mudclasts up to 20 cm in diameter	Sharp	-	Slumping of heterolithic packages
<b>LF12</b> Mudstone	Mudstone or very fine siltstone	Ungraded or slightly graded	1 - 16 cm (locally up to 30 cm)	Massive, occasionally finely laminated	None	Sharp or gradational with underlying strata	T <sub>d</sub> , T <sub>e</sub>	Deposition en masse or incrementally, by floc segregation settling and fallout from dilute low-density turbidity currents

Table 1

ELEMENTARY CHANNEL ARCHITECTURE	WIDTH (m)	THICKNESS (m)	ASPECT RATIO	CHANNEL FILL FACIES	OUT-OF-CHANNEL FACIES
<b>Weakly-confined Channels</b>	> 450	9 – 17	> 50	<p><b>Axis:</b> LF2B</p> <p><b>Margins:</b> LF2A and LF3 alternating with thin mudstones (LF12)</p> <p><b>Above basal surface:</b> LF1B (rare LF1A)</p>	<p><b>Proximal:</b> Sand-prone (F.A.2)</p> <p><b>Distal:</b> Mud-prone (F.A.3)</p>
<b>Incisional Channels</b>	180 - 450	13 - 26	13 - 30	<p><b>Axis:</b> LF2B</p> <p><b>Margins:</b> LF2B; LF2A and LF3 alternating with thin mudstones (LF12) in proximity of the channelform edges</p> <p><b>Above basal surface:</b> LF1A - LF1B</p>	Mud-prone (F.A.3)

Table 2